INL/EXT-19-53812

# Determination of the Deuterium-Tritium (D-T) Generator Neutron Flux using Multi-foil Neutron Activation Analysis Method

D. Lee
B. Bucher
K. Krebs
E. Seabury
J. Wharton

July 2018


The INL is a U.S. Department of Energy National Laboratory
operated by Battelle Energy Alliance

INL/EXT-19-53812

# Determination of the Deuterium-Tritium (D-T) Generator Neutron Flux using Multi-foil Neutron Activation Analysis Method

**D. Lee**
**B. Bucher**
**K. Krebs**
**E. Seabury**
**J. Wharton**

**July 2019**

**Idaho National Laboratory**
**Nuclear Nonproliferation Division**
**Idaho Falls, Idaho 83415**

**http://www.inl.gov**

**Prepared for the**
**U.S. Department of Energy**
**Office of National Nuclear Security Administration**
**Under DOE Idaho Operations Office**
**Contract DE-AC07-05ID14517**

# ABSTRACT

The deuterium-tritium (D-T) neutron flux from a Thermo-Fisher™ MP320 neutron generator was determined experimentally in this study. Fast neutron flux from a neutron generator can be measured indirectly using multi-foil activation analysis. Two sets of 12 activation foils each were prepared to cover a broad energy range of fast neutrons (1 – 15 MeV), and spectral peak analysis was performed on each activated foil with a mechanically-cooled HPGe detector. A non-negative solution of a linear least squares problem was solved to find a neutron flux energy distribution. The neutron yields of the high-yield (60 μA−90 kV) and low-yield (30 μA−70 kV) settings were determined to be $1.73\times10^{8}$ n/s and $2.28\times10^{7}$ n/s, respectively. Uncertainties on these neutron yields were estimated using the BC400 scintillator count rates whose fluctuations throughout the irradiations were described by the standard deviations of 10.6 and 8.5%, respectively. Linear relationships between the MP320's neutron flux and a BC400 scintillator as well as a SWENDI-2 neutron dose meter were also derived to utilize them as on-line neutron flux monitors in the future.

# CONTENTS



# FIGURES

## TABLES

# ACRONYMS

| | |
|---|---|
| COTS | Commercial off-the-shelf |
| D-T | Deuterium-tritium |
| GB | Sarin nerve agent |
| GOTS | Government off-the-shelf |
| HD | Sulfur mustard blister agent |
| HPGe | High purity germanium |
| INL | Idaho National Laboratory |
| L | Lewisite blister agent |
| MCNP | Monte Carlo n-particle |
| NNLS | Non-negative least squares |
| NNWLS | Non-negative weighted least squares |
| nROI | Neutron region of interest |
| PINS | Portable Isotopic Neutron Spectroscopy |
| VX | Nerve agent |

# Determination of the Deuterium-Tritium (D-T) Generator Neutron Flux using Multi-foil Neutron Activation Analysis Method

## 1. MULTI-FOIL ACTIVATION ANALYSIS METHOD

Fast neutron flux from a neutron generator can be measured indirectly using multi-foil activation analysis. Multiple activation foils are selected to cover a broad energy range of fast neutrons. The half-lives, isotopic branching ratios and resulting intensities of emitted gamma-rays after activation are essential factors in selecting what type of foil to activate. If the half-lives of the activated isotopes are too short, not many activated nuclei survive to the beginning of the counting. Also, intensities (branching ratios) and energies of characteristic gamma-rays emitted from activated nuclei must be suitable to accumulate enough net counts above background to be detected during gamma-ray spectroscopy. Once an activation foil is attached to the surface of a neutron generator, it is exposed to fast neutrons for an irradiation time of $\boldsymbol{t_{irr}}$. Then, an energy calibrated HPGe detector with known absolute detection efficiency counts gamma-rays emitted from the activation foil for a real counting time of $\boldsymbol{t_c}$. A delay time of $\boldsymbol{t_d}$ between the end of the irradiation and the beginning of the counting is recorded as well. Once the net count $\boldsymbol{N_i}$ of a full energy gamma-ray peak at $\boldsymbol{E_i}$ from an activated isotope is obtained from the spectral peak analysis, it is related to the other measured quantities and the neutron spectrum, $\boldsymbol{\varphi(E)}$, by

$$
\begin{aligned}
N_i &\approx C_i \times \sum_{j=1}^{n} \sigma_{i,j}\varphi_j \\
&= A_i \times f_{time} \times f_{self} \times f_{spec} \times \sum_{j=1}^{n} \sigma_{i,j}\varphi_j \\
&= A_i \times \left[\frac{\left(1-e^{-\lambda_i t_{irr}}\right)\times e^{-\lambda_i t_d}\times\left(1-e^{-\lambda_i t_c}\right)}{\lambda_i}\times\left(\frac{t_{live}}{t_c}\right)\right]\times\left[\frac{1-e^{-\mu(E_i)\rho_i x_i}}{\mu(E_i)\rho_i x_i}\right] \\
&\qquad \times [\varepsilon(E_i)\times BR(E_i)]\times\sum_{j=1}^{n}\sigma_{i,j}\varphi_j
\end{aligned}
\tag{1}
$$

where $i$ = the index number of a gamma-ray peak,
$j$ = the index number of the $j^{th}$ energy bin ($j = 1, \cdots, n$),
$E_i$ = $i^{th}$ gamma-ray's energy [keV],
$N_i$ = the net count of $i^{th}$ gamma-ray peak at $E_i$ [counts],
$A_i$ = the number of isotopes in the activation foil to emit gamma-rays at $E_i$ [#],
$\sigma_{i,j}$ = the cross section in the $j^{th}$ energy bin to produce the activated isotopes that emits gamma-rays at $E_i$ [cm$^2$],
$\varphi_j$ = the discrete neutron flux in the $j^{th}$ energy bin [n/cm$^2$/s],
$\varepsilon(E_i)$ = an HPGe detector's absolute detection efficiency for gamma-rays at $E_i$,
$BR(E_i)$ = the absolute intensity (branching ratio) of gamma-rays at $E_i$ from the activated isotopes,
$\lambda_i$ = decay constant of the activated isotopes that emit gamma-rays at $E_i$ with $BR(E_i)$ [s$^{-1}$],

$t_{irr}$ = irradiation time [s],
$t_d$ = delay time between the end of the irradiation and the start of the counting [s]
$t_{live}$ = live counting time [s],
$t_c$ = real counting time [s],
$\mu(E_i)$ = material dependent mass attenuation coefficient as a function of photon of energy $E_i$ [cm$^2$/g],
$\rho_i$ = the activation foil's density [g/cm$^3$], and
$x_i$ = target foil's thickness [cm].

$f_{time}$ is a time correction factor to take into account decay of the activated isotopes through the irradiation, transfer and counting and dead time correction. $f_{self}$ is a correction factor of gamma-ray self-attenuation in the foil. This factor becomes non-negligible when the foil thickness increases and gamma-ray energy decreases. $f_{spec}$ is a spectroscopic factor to account for the branching ratio and the absolute detection efficiency. In **EQUATION (1),** the neutron flux is the only unknown to be solved while all the other quantities are either known or measured. The neutron flux's energy resolution (the number of $j$) is limited by the number of $i$ although an ill-defined problem might be solved numerically at the cost of uncertainty. Therefore, it is favorable to include as many characteristic gamma-ray peaks with decent intensities as possible from multiple activation foils. If $m$ unique gamma-ray peaks ($i = 1, 2, \cdots, m$) are used to find a $n$-group neutron spectrum ($j = 1, 2, \cdots, n$), **EQUATION (1)** in a matrix form is given by

$$\begin{bmatrix} N_1 \\ N_2 \\ \vdots \\ N_{m-1} \\ N_m \end{bmatrix} = \begin{bmatrix} C_1 & 0 & \cdots & 0 & 0 \\ 0 & C_2 & & 0 & 0 \\ \vdots & & \ddots & \vdots & \\ 0 & 0 & \cdots & C_{m-1} & 0 \\ 0 & 0 & & 0 & C_m \end{bmatrix} \times \begin{bmatrix} \sigma_{1,1} & \sigma_{1,2} & \cdots & \sigma_{1,n-1} & \sigma_{1,n} \\ \sigma_{2,1} & \sigma_{2,2} & & \sigma_{2,n-1} & \sigma_{2,n} \\ \vdots & & \ddots & \vdots & \\ \sigma_{m-1,1} & \sigma_{m-1,2} & \cdots & \sigma_{m-1,n-1} & \sigma_{m-1,n} \\ \sigma_{m,1} & \sigma_{m,2} & & \sigma_{m,n-1} & \sigma_{m,n} \end{bmatrix} \times \begin{bmatrix} \varphi_1 \\ \varphi_2 \\ \vdots \\ \varphi_{n-1} \\ \varphi_n \end{bmatrix} \quad (2)$$

**EQUATION (2)** can be solved numerically to find the *n*-group neutron flux, which requires inversion of a non-square matrix. There are a few methods to solve this kind of problems with the constraints of non-negative $\varphi_j$ values. Non-negative Least Squares (NNLS) or Non-negative Weighted Least Squares (NNWLS) can be performed in MATLAB® or OCTAVE to solve **EQUATION (2)** [Mat18, Oct18]. Also, a solution of **EQUATION (2)** can be obtained in the Microsoft Excel using the solver add-in as an optimization problem, but a good initial guess of $\boldsymbol{\varphi}$ vector in **EQUATION (2)** is required to find a converged realistic solution, and neutron spectra from similar studies could be used as an initial guess for fast convergence to a solution.

## 2. EXPERIMENTS

The deuterium-tritium (D-T) neutron flux from a Thermo-Fisher™ MP320 neutron generator was determined by the multi-foil activation analysis method described in the previous section. In order to cover a broad range (1 – 15 MeV) of neutron energies, a fast neutron foils kit (SWX-1551 fast neutron kit plus a pair of Nb foils) was purchased from Shieldwerx™ [Shi18]. **TABLE 1** summarizes some fast neutron induced reactions with the foils included in this kit. The kit includes two foils per each element as shown in **FIGURE 1**, and the foils come in the form of thin 0.5" diameter discs whose thicknesses and sample masses are summarized in **TABLE 2**. One exception is that sodium and chlorine activations were done with

the NaCl compound discs in the kit. Sulfur foils were not used in this experiment as activated sulfur isotopes are mostly pure β-emitters. Reaction cross sections listed in the **TABLE 1** are plotted over a range of neutron energies from 1 to 15 MeV in **FIGURE 2**.

An MP320 D-T neutron generator was set up in the south cave of the PINS lab. The generator's tritium target plane was located at 91 cm above the concrete floor. The foils were placed inside polyethylene bags and attached to the surface of the generator centered on the generator's target plane. The distance between the foil and the center of the tritium target was measured as 5.08 cm, which is equal to the radius of the generator around the target plane. Each foil was irradiated for at least 6 hours. During irradiation, a 2.54-cm x 1.27-cm plastic scintillator was added as an independent neutron flux monitor. It was placed 50 cm away from the surface of the generator and at 91 cm above the floor. Accumulated neutron spectrum from BC400 was also saved every hour during the irradiation. The neutron counts in the plastic scintillator could be calibrated to the neutron flux determined from the activation analysis, and then it could be used as a real-time stand-alone neutron flux monitor in the future. This procedure was repeated for all 12 foils. **FIGURE 3** and **4** shows schematic diagrams of the irradiation setup, and the actual experimental setup in the south cave of the PINS lab.

Once irradiation was complete, the foil was transferred to a low-background counting area outside the irradiation cave where a mechanically cooled HPGe detector collected a passive gamma-ray spectrum for 12 hours or longer. An accumulated gamma-ray spectrum of each foil was saved every hour. Two identical sets of 12 foils were prepared to be activated under two different generator operation settings. The first set of 12 foils were irradiated with the generator operated at its maximum setting, 60 μA−90 kV (high-yield), emitting on the order of $1\times10^8$ n/s. The neutron generator was run at 30 μA−70 kV (low-yield) during the second set of irradiations. This setting was chosen to yield an estimated $1\times10^7$ n/s.

**TABLE** 3 summarizes each foil's irradiation, real and live counting and delay times.

# 3. DATA ANALYSIS

## 3.1 HPGe absolute detection efficiency

**EQUATION (1)** requires that an HPGe detector's absolute full energy peak efficiency should be known as a function of gamma-ray energy. Therefore, an absolute efficiency function at a fixed counting position with an ORTEC®'s IDM detector [Ort18] was determined before activating any foils. A newly purchased mixed calibration source with multiple radioisotopes was used for the efficiency measurements. The mixed source is a disc of 54 mm in diameter and 3 mm in thickness, and its active source area is 10 mm in diameter. The mixed calibration source was calibrated on January 1st 2018 by the manufacturer, and its certificate provided the emission rates of the characteristic gamma-rays at the time of the calibration. For a gamma-ray full energy peak at $E_i$ from a radioisotope $k$, absolute full energy peak efficiency $\varepsilon(E_i)$ is calculated by

$$\varepsilon(E_i) = \frac{N(E_i)}{(r_i \times e^{-\lambda_k \Delta t}) \times \frac{(1-e^{-\lambda_k t_c})}{\lambda_k} \times \left(\frac{t_{live}}{t_c}\right)} = \frac{N(E_i)}{R(E_i)} \qquad (3)$$

where $N(E_i)$ = net count under the full energy peak at $E_i$,

$R(E_i)$ = a total number of emitted gamma-rays at $E_i$ from a radioisotope $k$,
$r_i$ = emission rate of gamma-ray at $E_i$ from a radioisotope $k$ at the time of the manufacturer's calibration [$s^{-1}$],
$\lambda_k$ = decay constant of a radioisotope $k$ that emits gamma-rays at $E_i$ [$d^{-1}$],
$\Delta t$ = elapsed time between the manufacturer's calibration and the beginning of new measurements [d],
$t_{live}$ = live counting time [s], and
$t_c$ = real counting time [s].

The source was attached to the endcap of the IDM01 detector whose energy calibration was already conducted at the time of the efficiency measurements. The mixed source emits 12 characteristic gamma-rays from 9 different radioisotopes to derive a continuous efficiency curve by fitting the data points with a function given by

$$\varepsilon(E) = exp\left(\sum_{l=0}^{4} a_l (ln(E))^l\right) \quad (4)$$

11 out of 12 characteristic gamma-rays were used in the analysis as shown in **Figure 5**. All measured and calculated quantities for **EQUATION (3)** are summarized in

Table 4, and the coefficients determined from the fitting with the function in **EQUATION (4)** are also listed. Later, all activated foils were counted exactly at the same position of the mixed source where the absolute efficiency function was derived from.

## 3.2 Gamma-ray Spectrum Analysis

Spectral peak analysis was performed on a collection of gamma-ray spectra for each foils set. As discussed in section 2, foils were divided into two sets to be activated under the generator's different operation settings, 60 μA−90 kV and 30 μA−70 kV. The IDM01 was operated to collect a background spectrum for 12 hours before the activation started. For each collection of gamma-ray spectra from the activated foils, spectral peak analysis was repeated on the gamma-ray peaks listed in **TABLE 1**. Each gamma-ray peak was fit with a Gaussian function on top of a linear baseline function after the time-normalized background spectrum was subtracted. **FIGURE 6** through **FIGURE 17** are gamma-ray spectra counted by the IDM01 after the irradiations under the high-yield setting. The spectra irradiated under the low-yield setting show the same structures overall, but gamma-ray peaks from the activated radioisotopes are not visible or much weaker than those from the high-yield setting because the neutron yield was reduced by an order of magnitude. Therefore, some gamma-ray peaks were not analyzed in the low-yield

setting. Also, it was much easier to analyze gamma-ray peaks from very short-lived radioisotopes in the first a few hours' spectra than full 12- or 24-hour spectra. For example, weak gamma-ray peaks from $^{37}$S ($T_{1/2}$ = 303 seconds) and $^{51}$Ti ($T_{1/2}$ = 346 seconds) were analyzed using the first hour's spectra. These peaks were completely masked by the background in the spectra with the longer counting times. **TABLE 5** summarizes results of the spectral analysis performed on the gamma-ray peaks listed in **TABLE 1**. The net counts, $N_i$, and the calculated coefficients, $C_i$, are listed for each D-T generator setting. Each reaction's cross-section from 1 to 15 MeV in increments of 1 MeV is tabulated in

Table 6.

### 3.2.1 Aluminum

Aluminum foils were irradiated for 6 hours and then counted for 12 hours. **FIGURE 6** shows the aluminum spectrum from the 60 μA−90 kV operation and the background spectrum. Naturally occurring Aluminum consists of 100% $^{27}$Al. *843.76/1014.52 keV* peaks from $^{27}$Al(n,p)$^{27}$Mg ($T_{1/2}$ = 9.458 minutes) [Jak08] and *1368.626/2754.007 keV* peaks from $^{27}$Al(n,α)$^{24}$Na ($T_{1/2}$ = 14.997 hours) [Och11, Rei01, Ger89] were analyzed to determine the neutron flux. These peaks are easily fit and analyzed as shown in **FIGURE 6**. Additionally, $^{27}$Al(n,2n)$^{26}$Al reaction emits *1808.65 keV* gamma-rays with a high branching ratio of 0.998, but $^{26}$Al's very long half-life ($T_{1/2}$ = 7.17e5 years) and relatively low cross-section excluded this reaction from the analysis.

### 3.2.2 Copper

Copper foils were irradiated for 6 hours and then counted for 12 hours. **FIGURE 7** shows the copper spectrum from the 60 μA−90 kV operation and the background spectrum. Naturally occurring copper consists of 69% $^{63}$Cu and 31% $^{65}$Cu. $^{63}$Cu and $^{65}$Cu have relatively large (n,2n) cross-sections above 9 MeV that make them ideal for the activation study with D-T neutrons. *511 keV* gamma-rays were emitted from both $^{63}$Cu(n,2n)$^{62}$Cu ($T_{1/2}$ = 9.673 minutes) [Jak08, Gha86] and $^{65}$Cu(n,2n)$^{64}$Cu ($T_{1/2}$ = 12.701 hours) [Gha86]. This issue could be easily solved by using isotopic $^{63}$Cu or $^{65}$Cu foils if available, but elemental copper foils can be used with an extra step in spectral peak analysis. At the beginning of the counting, *511 keV* gamma-ray peak is dominated by $^{62}$Cu, but nearly all $^{62}$Cu dies away after 8 hours due to a very short half-life of 580 seconds. Therefore, the data from the last four-hours are almost free from the contributions from the short-lived $^{62}$Cu. As a result, *511/1345.77 keV* peaks from $^{64}$Cu were analyzed to derive neutron flux.

### 3.2.3 Iron

Iron foils were irradiated for 6 hours and then counted for 12 hours. **FIGURE 8** shows the iron spectrum from the 60 μA−90 kV operation and the background spectrum. The *846.76/1810.73/2113.09 keV* peaks from $^{56}$Fe(n,p)$^{56}$Mn ($T_{1/2}$ = 2.5789 hours) [Bar95] were analyzed to determine the neutron flux. There are *2657.56/2959.92/3369.81 keV* peaks reported from the same reaction, but their branching ratios are too small to be useful. $^{54}$Fe(n,p)$^{54}$Mn ($T_{1/2}$ = 312.2 days) [Zol13] seems ideal to determine the downscattered D-T neutron flux thanks to its relatively large cross-section from 3 to 13 MeV, but $^{54}$Mn's very long half-life of 312.2 days make this reaction less useful in this study. Also, $^{56}$Fe(n,α)$^{51}$Cr reaction is less important due to $^{51}$Cr's long half-live of 27.7025 days.

### 3.2.4 Titanium

Titanium foils were irradiated for 8 hours and then counted for 24 hours. ERROR! REFERENCE SOURCE NOT FOUND. shows the titanium spectrum from the 60 μA−90 kV operation and the background spectrum. Reaction products from titanium are mostly long-lived radioisotopes with half-lives over a few days, and $^{48}$Ti is probably the best titanium isotope to be used in the activation analysis thanks to its high natural abundance of 74%. The other titanium isotopes suffer from low abundance of less than 10%. The *159.381 keV* peak from $^{47}$Ti(n,p)$^{47}$Sc ($T_{1/2}$ = 3.3492 days) [Voy17] and *983.526/1037.522/175.361/1312.12 keV* peaks from $^{48}$Ti(n,p)$^{48}$Sc ($T_{1/2}$ = 43.67 hours) were analyzed to determine the neutron flux.

### 3.2.5 Indium

Indium foils were irradiated for 8 hours and then counted for 24 hours. **FIGURE 10** shows the indium spectrum from the 60 μA−90 kV operation and the background spectrum. $^{115}$In is very promising isotope especially for the D-T neutron activation analysis because of its high abundance and large (n,2n) cross-sections above 9 MeV. Also, $^{115}$In(n,n')$^{115m}$In ($T_{1/2}$ = 4.486 hours) and $^{115}$In(n,γ)$^{116m}$In ($T_{1/2}$ = 54.29 minutes) are good indicator for D-D neutrons and neutrons below 1 MeV, respectively, due to their large cross sections as shown in **FIGURE 2**. The *558.43/190.27 keV* peaks from $^{115}$In(n,2n)$^{114m}$In ($T_{1/2}$ = 49.51 days) [Men69], *336.241 keV* peak from $^{115}$In(n,n')$^{115m}$In [Och11, Men69], and *1293.56/1097.28 keV* peaks from $^{115}$In(n,γ)$^{116m}$In [Bla10] were analyzed to determine the neutron flux.

### 3.2.6 Nickel

Nickel foils were irradiated for 8 hours and then counted for 24 hours. **FIGURE 11** shows the nickel spectrum from the 60 μA−90 kV operation and the background spectrum. $^{58}$Ni(n,p)$^{58}$Co reaction [Och11, Bar95] is ideal to determine the downscattered D-T neutron flux thanks to its relatively large cross-section over a broad energy range from 3 to 13 MeV. Analyzed gamma-ray peaks from nickel foils were from activation of $^{58}$Ni whose natural abundance is 68%. *810.7593 keV* peak from $^{58}$Ni(n,p)$^{58}$Co ($T_{1/2}$ = 70.86 days), *1377.63/1757.55/1919.52 keV* peaks from $^{58}$Ni(n,2n)$^{57}$Ni ($T_{1/2}$ = 35.6 hours) [Bar95], and *122.0607/136.4736 keV* peaks from $^{58}$Ni(n,np or d)$^{57}$Co ($T_{1/2}$ = 271.74 days) [Plo02] were analyzed to determine the neutron flux.

### 3.2.7 Sodium Chloride

Sodium Chloride foils were irradiated for 6 hours and then counted for 12 hours. **FIGURE 12** shows the sodium chloride spectrum from the 60 μA−90 kV operation and the background spectrum. No reaction products on $^{23}$Na were identified to yield gamma-ray peaks suitable for the activation analysis in this study. Naturally occurring chlorine consists of 76% $^{35}$Cl and 24% $^{37}$Cl. The *146.36 keV* peak from $^{35}$Cl(n,2n)$^{34m}$Cl ($T_{1/2}$ = 32 seconds) [Fes00] and the *3103.37 keV* peak from $^{37}$Cl(n,p)$^{37}$S ($T_{1/2}$ = 5.05 minutes) [Fes00] were analyzed to determine the neutron flux. It should be noted that only the first hour of data were used to analyze the *3103.37 keV* peak from $^{37}$S whose half-life is merely 303 seconds. This peak was also found to have poor counting statistics due to low detection efficiency.

### 3.2.8 Vanadium

Vanadium foils were irradiated for 8 hours and then counted for 24 hours. **FIGURE 13** shows the vanadium spectrum from the 60 μA−90 kV operation and the background spectrum. The *320.076 keV* peak from $^{51}$V(n,p)$^{51}$Ti ($T_{1/2}$ = 5.76 minutes) [Rei01, Fes00] and *983.526/1312.12/1037.522 keV* peaks from $^{51}$V(n,α)$^{48}$Sc ($T_{1/2}$ = 43.67 hours) [Rei01] were analyzed to determine the neutron flux. It should be noted

that the first hour of data were used to analyze the *320.076 keV* peak from $^{51}$Ti whose half-life is only 346 seconds.

### 3.2.9 Zinc

Zinc foils were irradiated for 6 hours and then counted for 12 hours. **FIGURE 14** shows the zinc spectrum from the 60 μA−90 kV operation and the background spectrum. The *669.62 keV* peak from $^{64}$Zn(n,2n)$^{63}$Zn ($T_{1/2}$ = 38.47 minutes) [Bha13, Voy17] and *438.634 keV* peak from $^{70}$Zn(n,2n) $^{69m}$Zn ($T_{1/2}$ = 13.756 hours) [Kel06] were analyzed to determine the neutron flux. $^{66}$Zn has relatively large (n,2n) cross-section above 9 MeV, but its low abundance of 28% and long half-life of 243.93 days prevented this isotope from being used in this study.

### 3.2.10 Magnesium

Magnesium foils were irradiated for 6 hours and then counted for 12 hours. **FIGURE 15** shows the magnesium spectrum from the 60 μA−90 kV operation and the background spectrum. The *1368.626/2754.007 keV* peaks from $^{24}$Mg(n,p)$^{24}$Na ($T_{1/2}$ = 14.997 hours) [Ger89] were analyzed to determine the neutron flux.

### 3.2.11 Zirconium

Zirconium foils were irradiated for 8 hours and then counted for 24 hours. **FIGURE 16** shows the zirconium spectrum from the 60 μA−90 kV operation and the background spectrum. The *202.53/479.51 keV* peaks from $^{90}$Zr(n,p)$^{90m}$Y ($T_{1/2}$ = 3.19 hours) [Mar90] and *909.15 keV* peak from $^{90}$Zr(n,2n)$^{89}$Zr ($T_{1/2}$ = 78.41 hours) [Och11, Bar95] were analyzed to determine the neutron flux. $^{90}$Zr is a suitable for the D-T neutron activation analysis because of its large (n,2n) cross-section above 9 MeV and its natural abundance of 51.45%.

### 3.2.12 Niobium

Niobium foils were irradiated for 8 hours and then counted for 24 hours. **FIGURE 17** shows the niobium spectrum from the 60 μA−90 kV operation and the background spectrum. The *202.53/479.51 keV* peaks from $^{93}$Nb(n,α)$^{90m}$Y ($T_{1/2}$ = 3.19 hours) [Hon10] and *934.44 keV* peak from $^{93}$Nb(n,2n)$^{92m}$Nb ($T_{1/2}$ = 10.15 days) [Och11] were analyzed to determine the neutron flux. $^{93}$Nb is an ideal isotope especially for the D-T neutron activation analysis because of its 100% abundance and large (n,2n) cross-section above 9 MeV.

## 3.3 Neutron flux

**EQUATION (2)** can be re-written to **EQUATION (5)** after combining the cross-sections with the coefficients.

$$N = C \cdot \sigma \cdot \varphi = X \cdot \varphi \tag{5}$$

When all quantities except the neutron flux were either measured or calculated, a built-in NNLS function in OCTAVE was used to find to solve **EQUATION (5)** to find a solution, $\boldsymbol{\varphi}$. In order to use NNWLS, **EQUATION (5)** must be modified further to include the weight matrix and a new equation is given by

$$N' = \sqrt{W}N = \sqrt{W}X \cdot \varphi = X' \cdot \varphi \tag{6}$$

where $\boldsymbol{W}$ is the diagonal matrix of weights whose element $w_i$ is equal to the reciprocal of the variance of the measured quantity $N_i$. Then, the NNLS function in OCTAVE was applied to the modified $\boldsymbol{N'}$ and $\boldsymbol{X'}$.

**FIGURE 18** shows the solved neutron fluxes for two generator settings, respectively. The determined neutron fluxes are peaked around 14 MeV as expected, and low energy room-return neutrons are present unlike a simulated neutron flux. Interestingly, there is another minor peak around 5-6 MeV whose origin is not clear. It is speculated that these neutrons could be the downscattered D-T neutrons off from certain structural components in the generator. However, this explanation is not strongly supported by other studies that have performed detailed Monte Carlo simulations. In **FIGURE 19**, simulated neutron fluxes from the same MP320 D-T generator are shown for comparison. Alexa and Uhlář conducted a MCNP simulation study of the MP320 generator, but no significant contributions from neutrons around 5-6 MeV were reported [Ale13]. More recently, Remetti et al. performed very sophisticated and realistic MCNP simulations of the same generator [Rem17], and their results are in good agreement with those from Alexa and Uhlář. These simulation results show that there are minor contributions from neutrons over the mid-energy range, but experimental multi-foil activation analysis coupled to numerical methods is not sensitive enough to neutrons of such minor contributions. Therefore, it is more likely that these peaks were numerically introduced to minimize least squares over a broad energy range from 2 to 13 MeV.

Finally, a neutron yield of 14.1 MeV neutrons, $\boldsymbol{Y}$, was calculated using the summed neutron flux above 13 MeV for each generator setting. The sum of neutron flux over 13 MeV was multiplied by the entire solid angle at 5.08 cm, the distance of the foils from the center of the generator. The neutron yields of the high-yield and low-yield settings were determined to be $1.73\times10^8$ n/s and $2.28\times10^7$ n/s, respectively. Uncertainties on these neutron yields were estimated using the BC400 count rates whose fluctuations throughout the irradiations were described by the standard deviations of 10.6 and 8.5%, respectively. Two previous studies have derived empirical formulae to predict the neutron yield as functions of the generator's current-voltage setting. Alexa and Uhlář suggested a simple equation by

$$Y\ [n/s] = 7060 \times D \times \left(I - \frac{V}{20}\right) \times (V - 40)^{3/2} \tag{7}$$

where $\boldsymbol{D}$ is the duty factor, $\boldsymbol{I}$ is the current in μA, and $\boldsymbol{V}$ is the voltage in kV. The neutron yields of the high-yield and low-yield settings ($\boldsymbol{D}$ = 1.0) using **EQUATION (7)** were determined to be $1.44\times10^8$ n/s and $3.28\times10^7$ n/s, respectively. Remetti et al. has suggested their own formulae as functions of voltage for 20, 40 and 60 μA, respectively, given by

$$Y\ [n/s] = \begin{cases} 194.6 \times V^3 - 20990 \times V^2 + 1.126\times10^6 \times V - 2.121\times10^7, & I = 20\mu A \\ -98.91 \times V^3 + 47970 \times V^2 - 2.960\times10^6 \times V + 5.371\times10^7, & I = 40\mu A \\ -148.4 \times V^3 + 71960 \times V^2 - 4.439\times10^6 \times V + 8.056\times10^7, & I = 60\mu A \end{cases} \tag{8}$$

The neutron yield of the high-yield setting from **EQUATION (8)** was calculated to be $1.56\times10^8$ n/s while the neutron yield of the low-yield setting was interpolated to be $3.46\times10^7$ n/s. Neutron yields from **EQUATION (8)** are subject to about 25% uncertainties according to the authors. **FIGURE 20** and **FIGURE 21** compares the neutron yields determined in this study to those from references. The neutron yield for the 60 μA−90 kV setting in this study is slightly higher than the references although they are all within each other's uncertainty. However, the neutron yield for the 30 μA−70 kV setting in this study is noticeably lower than the references. In **FIGURE 21**, it is shown that the neutron yield for 30 μA−70 kV setting in this study is in better agreement with those at 20 μA−70 kV setting predicted by the references.

Table 7. Summary of neutron yields. Neutron yields are given in the unit of n/s. summarizes the estimated neutrons yields for voltages from 40 kV to 100 kV and currents from 20 μA to 60 μA, using **EQUATION (7)** and **(8)**, respectively. The neutron yields determined in this study are also shown in the last two columns of

Table 7. Summary of neutron yields. Neutron yields are given in the unit of n/s. for comparison.

## 3.4 BC400 plastic scintillator

A Bicron® BC400 [Sai18] scintillation detector shown in **FIGURE 22** was used as an independent neutron flux monitor during irradiations. Its position has remained at the same location specified in **FIGURE 3**, and its accumulated spectrum was saved every hour to create a time series of the hourly count rates. A typical neutron spectrum from an irradiation along with the background spectrum are shown in **FIGURE 23**. The generator was turned off to collect the background spectrum, and only natural gamma-rays and neutrons contributed to the recorded counts. Neutrons from the generator dominate the spectrum when the generator is turned on to activate foils, but high-energy gamma-rays from neutron-induced reactions must be taken into account. However, counts in the shaded region (labelled as "nROI") in **FIGURE 23** are most likely from 14.1 MeV neutrons although minor contributions from high-energy gamma-rays are still present as background counts. A prior research suggested that a region above natural background in the

BC400 spectra should be used to monitor neutron flux as counts in this region are insensitive to any gamma-rays induced by 14.1 MeV neutrons [Mit08]. Therefore, a neutron region of interest (nROI) was set up to integrate the hourly 14.1 MeV neutron count rate. The scintillator was not energy calibrated for this study so that the x-axis unit in **FIGURE 23** is given in keV electron equivalent [keVee] from the MCA's stored settings for gamma-rays. Therefore, it should be noted that the energy range of the nROI from 1132 to 1248 keVee in this study is for indicative purposes only, not for true neutron energies. The average hourly count rate within the nROI was recorded for each foil's 6- or 8-hour irradiation, and a time series over a two-month period is shown in **FIGURE 24**. Also, a 65-hour continuous operation of the same generator was performed at the end of the experiments. The average nROI count rates for two generator settings were $1.36\times10^5$ nROI counts/hour and $1.34\times10^4$ nROI counts/hour, respectively. There was noticeable decreases in hourly count rates for the high-yield setting, and the standard deviation of the observed count rates was found to be 10.6% of the average value. For the low-yield setting, the standard deviation was about 8.5% of the average. These decreases in the count rates were used to estimate the uncertainties of the determined neutron yields as described in SECTION NEUTRON flux. Eventually, this BC400 scintillator can be used as a neutron yield monitor for D-T neutron generators in the future. A correlation function between nROI hourly count rates and MP320 D-T neutron yields was derived from the first-order approximation and is given by

$$Y\,[n/s] = 1.23\times10^3 \times nROI\,[counts/hr] + 5.85\times10^6 \tag{9}$$

However, it is important to understand that **EQUATION (9)** is not universal to be applied to any combination of a BC400 and neutron generator. This equation is valid only when a BC400 is calibrated to perform identically to the one used in this study and its distance from a D-T generator is the same as shown in **FIGURE 3**.

## 3.5 SWENDI-2

As another candidate for a neutron yield monitor, a SWENDI-2 [Ols00, The18] neutron dose meter was used to derive a correlation function between its dose rates and neutron yields as shown in **FIGURE 25**. The SWENDI-2 was vertically centered at the same height of the generator's target plane (91 cm above the floor) and 100 cm distant from the surface of the generator. The measurements were repeated for 88 different generator settings: voltage was varied from 40 kV to 90 kV in increments of 5 kV while current was varied from 25 μA to 60 μA in increments of 5 μA. Ten 30-second dose rate readings were collected for each generator setting. Then, these ten readings were averaged to be a nominal value for each setting as summarized in **TABLE 8**. A graph of dose rate readings summarized in **TABLE 8** is shown in **FIGURE 26**. A correlation function between dose readings and MP320 D-T neutron yields was derived from the first-order approximation and is given by

$$Y\,[n/s] = 1.11\times10^6 \times Dose\ rate[mrem/hr] + 7.19\times10^5 \tag{10}$$

As with the BC400 scintillator, it should be noted that **EQUATION (10)** is only valid when a SWENDI-2 is calibrated to perform identically to the one used in this study and its distance from any MP320 D-T generator is set at 100 cm.

# 4. Discussion and Conclusion

Multi-foil activation analysis method was applied to determine the D-T neutron yield from a Thermo-Fisher™ MP320 neutron generator. Two sets of 12 foils each were activated under the generator's two operation settings, respectively. For the high-yield setting (60 μA−90 kV), the neutron yield of $1.73\times10^{8}$ n/s was determined by spectral peak analysis coupled to the weighted least squares method with non-negativity constraints. This neutron yield is about 10% higher than those from two previous studies on the same neutron generator model, but they are within error bars. This procedure was repeated for the second foil set, activated at 30 μA−70 kV, resulting in a determined neutron yield of $2.28\times10^{7}$ n/s, about 30% lower than predicted by the previous studies.

It is concerning that the monitored neutron yields from the BC400 were gradually decreasing with the standard deviation of as much as 10.6% at 60 μA−90 kV, but this setting is near the maximum operating condition suggested by the manufacturer, and it is expected that less than 10% standard deviation in the neutron yields would be observed under typical operating conditions. Also, it is possible that this issue might be actually related to the BC400 scintillator and the nROI approach.

It is interesting that there are not many studies that have characterized the MP320 D-T generator although this model is commonly used in many applications as a Commercial off-the-shelf (COTS) or Government off-the-shelf product (GOTS). This study was intended to determine the D-T neutron yield coming from a MP320 D-T generator, but it is speculated that further studies involving modeling and simulation could provide valuable information to the nuclear science community.

# REFERENCES


[Ale13] P. Alexa and R. Uhlář, "The first test of the new neutron generator at the VŠB – Technical university of Ostrava", GeoScience Engineering, vol. LIX, no.3, 2013, p.1

[Bar95] C. W. Barnes, A. R. Larson, G. LeMunyan, and M. J. Loughlin, Rev. Sci. Instrum. 66, 888 (1995)

[Bha13] C. Bhatia, W. Tornow, Measurement of the $^{64}Zn(n,2n)^{63}Zn$ reaction cross section between 12.5

and 14.5 MeV J. Phys. G, 40 (2013), p. 065104

[Bla10] J. Blachot, "Nuclear Data Sheets for A = 116", Nuclear Data Sheets 111 (3) (2010) 717–895

[Fes00] A. Fessler, A.J.M. Plompen, D.L. Smith, J.W. Meadows, Y. IkedaNeutron activation cross section measurements from 16 to 20 MeV for isotopes of F, Na, Mg, Al, Si, P, Cl, Ti, V, Mn, Fe, Nb, Sn, and BaNucl. Sci. Eng., 134 (2000), pp. 171-200

[Ger89] L.P. Geraldo, D.L. Smith, J.W. Meadows, "Activation cross section measurements near threshold for the $^{24}$Mg(n,p)$^{24}$Na and $^{27}$Al(n, α)$^{24}$Na reactions", Annals of Nuclear Energy, 16 (1989), p. 293

[Gha86] F. Ghanbari, J.C. Robertson, "The $^{63}$Cu(n,2n)$^{62}$Cu and $^{65}$Cu(n,2n)$^{64}$Cu cross sections at 14.8 MeV",Ann. Nucl. Energy, 13 (1986), pp. 301-306

[Hon10] Honusek M, Bém P, Fischer U, Götz M, Novák J, Simakov SP, Šimečková E, "The cross-section data from neutron activation experiments on niobium in the NPI p-$^{7}$Li quasi-monoenergetic neutron field", J Korean Phys Soc 59(2):1374–1377 (2010)

[Jak08] S. Jakhar, C. V. S. Rao, A. Shyam and B. Das, "Measurement of 14 MeV neutron flux from DT neutron generator using activation analysis," *2008 IEEE Nuclear Science Symposium Conference Record*, Dresden, Germany, 2008, pp. 2335-2338

[Kel06] Kelley, K., Hoffman, R.D., Dietrich, F.S., and Mustafa, M.G., "Neutron induced cross sections for radiochemistry for isotopes of nickel, copper, and zinc", UCRL-TR-221759, LLNL (2006).

[Mar90] A. Marcinkowski, U. Garuska, H.M. Hoang, D. Kielan, B. ZwieglinskiCross sections of the (n, p) reaction on zirconium isotopes Nucl. Phys. A, 510 (1990), p. 93

[Mat18] https://www.mathworks.com/help/matlab/ref/lsqnonneg.html

[Men67] H.O. Menlove, K.L. Coop, H.A. Grench et al., "Activation Cross Sections for the 19F(n,2n)18F, 23Na(n,2n)22Na, 55Mn(n,2n)54Mn, $^{115}$In(n,2n)$^{114m}$In, 165Ho(n,2n)164mHo, $^{115}$In(n,n')$^{115m}$In, and $^{27}$Al(n,α) $^{24}$Na reactions," Phys. Rev., 163, 1308 (1967).

[Mit08] S. Mitra and L. Wielopolski, Monitoring Neutron Generator Output in a Mixed Neutron-Gamma Field Using a Plastic Scintillator, BNL-80144-2008-CP, 2008

[Och11] K. Ochiai et al., "Neutron flux measurements in ITER-TBM simulating assemblies by means of multi-foil activation method", *Prog. Nucl. Sci. Technol.*, vol. 1, pp. 142-145, Feb. 2011

[Oct18] https://octave.sourceforge.io/octave/function/lsqnonneg.html

[Ols00] R. H. Olsher, H.-H. Hsu, A. Beverding, J. H. Kleck, W. H. Casson, D. G. Vasilik, and R. T. Devine, "WENDI: An improved neutron rem meter", Health Physics, vol.79, no.2, 2000, pp.170-181

[Ort18] https://www.ortec-online.com/products/radiochemistry-health-physics-research-industrial/gamma- spectroscopy/all-in-one-spectrometers/idm-200-v

[Plo02] A. J. M. Plompen, D. L. Smith, P. Reimer, S. M. Qaim, V. Semkova, F. Cserpak, V. Avrigeanu,

and S. Sudar, J. Nucl. Sci. Technol. Suppl. **2**, 192 (2002)

[Rei01] P. Reimer, PhD Thesis, Cologne University, Germany (2001)

[Rem17] R. Remetti, et al., "Development and Experimental Validation of a Monte Carlo Modeling of the Neutron Emission from a DT Generator", NIM A 842, 2017, pp.7-13

[Sai18] https://www.crystals.saint-gobain.com/products/bc400-bc404

[Shi18] http://www.shieldwerx.com/activation-foils.html

[The18] https://www.thermofisher.com/order/catalog/product/FHT762WENDI2

[Voy17] Voyles A., et al., "Measurement of the $^{64}$Zn, $^{47}$Ti(n,p) cross sections using a DD neutron generator for medical isotope studies", Nucl. Instrum. Methods Phys. Res. B, 410 (2017), pp. 230-239

[Zol13] Zolotarev, K.I., & Zolotarev, P.K. (2013). Evaluation of Some (n,n'), (n,γ), (n,p), (n,2n) and (n,3n) Reaction Excitation Functions for Fission and Fusion Reactor Dosimetry Applications; Evaluation of the Excitation Functions for the $^{54}$Fe(n,p)$^{54}$Mn, $^{58}$Ni(n,2n)$^{57}$Ni, $^{67}$Zn(n,p)$^{67}$Cu, $^{92}$Mo(n,p)$^{92m}$Nb, $^{93}$Nb(n,γ)$^{94}$Nb, $^{113}$In(n,n')$^{113m}$In, $^{115}$In(n,γ) $^{116m}$In, and $^{169}$Tm(n,3n)$^{167}$Tm Reactions Progress Report on Research Contract No 16242 (INDC(NDS)--0657). International Atomic Energy Agency (IAEA)

Table 1. A list of fast neutron induced reactions with signature gamma-rays to be analyzed.

| Isotope | Abundance [%] | Δ Abundance [%] | Reaction | $T_{1/2}$ [s] | Δ $T_{1/2}$ [s] | Eγ [keV] | Δ Eγ [keV] | BR | Δ BR |
|---|---|---|---|---|---|---|---|---|---|
| $^{27}$Al | 100.000 | 0.000 | $^{27}$Al(n,p)$^{27}$Mg | 567.48 | 0.72 | 843.76 | 0.1 | 0.718 | 0.0002 |
| $^{27}$Al | 100.000 | 0.000 | $^{27}$Al(n,p)$^{27}$Mg | 567.48 | 0.72 | 1014.52 | 0.1 | 0.28 | 0.0002 |
| $^{27}$Al | 100.000 | 0.000 | $^{27}$Al(n,a)$^{24}$Na | 53989.2 | 43.2 | 1368.626 | 0.005 | 0.999936 | 0.000015 |
| $^{27}$Al | 100.000 | 0.000 | $^{27}$Al(n,a)$^{24}$Na | 53989.2 | 43.2 | 2754.007 | 0.011 | 0.99855 | 0.00005 |
| $^{63}$Cu | 69.150 | 0.150 | $^{63}$Cu(n,2n)$^{62}$Cu | 580.38 | 0.48 | 511 | - | 1.9566 | 0.0005 |
| $^{65}$Cu | 30.850 | 0.309 | $^{65}$Cu(n,2n)$^{64}$Cu | 45723.6 | 7.2 | 511 | - | 0.352 | 0.004 |
| $^{65}$Cu | 30.850 | 0.309 | $^{65}$Cu(n,2n)$^{64}$Cu | 45723.6 | 7.2 | 1345.77 | 0.06 | 0.00475 | 0.00011 |
| $^{56}$Fe | 91.754 | 0.036 | $^{56}$Fe(n,p)$^{56}$Mn | 9284.04 | 0.36 | 846.7638 | 0.0019 | 0.9885 | - |
| $^{56}$Fe | 91.754 | 0.036 | $^{56}$Fe(n,p)$^{56}$Mn | 9284.04 | 0.36 | 1810.726 | 0.004 | 0.269 | 0.004 |

| | | | | | | | | | |
|---|---|---|---|---|---|---|---|---|---|
| $^{56}$Fe | 91.754 | 0.036 | $^{56}$Fe(n,p)$^{56}$Mn | 9284.04 | 0.36 | 2113.092 | 0.006 | 0.142 | 0.003 |
| $^{47}$Ti | 7.440 | 0.020 | $^{47}$Ti(n,p)$^{47}$Sc | 289370.9 | 51.84 | 159.381 | 0.015 | 0.683 | 0.004 |
| $^{48}$Ti | 73.720 | 0.030 | $^{48}$Ti(n,p)$^{48}$Sc | 157212 | 324 | 983.526 | 0.012 | 1.001 | 0.006 |
| $^{48}$Ti | 73.720 | 0.030 | $^{48}$Ti(n,p)$^{48}$Sc | 157212 | 324 | 1037.522 | 0.012 | 0.976 | 0.007 |
| $^{48}$Ti | 73.720 | 0.030 | $^{48}$Ti(n,p)$^{48}$Sc | 157212 | 324 | 175.361 | 0.005 | 0.0748 | 0.001 |
| $^{48}$Ti | 73.720 | 0.030 | $^{48}$Ti(n,p)$^{48}$Sc | 157212 | 324 | 1312.12 | 0.012 | 1.001 | 0.007 |
| $^{115}$In | 95.710 | 0.050 | $^{115}$In(n,2n)$^{114m}$In | 4277664 | 8640 | 558.43 | 0.03 | 0.044 | 0.006 |
| $^{115}$In | 95.710 | 0.050 | $^{115}$In(n,2n)$^{114m}$In | 4277664 | 8640 | 190.27 | 0.03 | 0.1556 | 0.0015 |
| $^{115}$In | 95.710 | 0.050 | $^{115}$In(n,n')$^{115m}$In | 16149.6 | 14.4 | 336.241 | 0.025 | 0.459 | 0.001 |
| $^{115}$In | 95.710 | 0.050 | $^{115}$In(n,γ)$^{116m}$In | 3257.4 | 10.2 | 1293.56 | 0.02 | 0.848 | 0.012 |
| $^{115}$In | 95.710 | 0.050 | $^{115}$In(n,γ)$^{116m}$In | 3257.4 | 10.2 | 1097.28 | 0.02 | 0.585 | 0.008 |
| $^{58}$Ni | 68.070 | 0.009 | $^{58}$Ni(n,p)$^{58}$Co | 6122304 | 5184 | 810.7593 | 0.002 | 0.9945 | - |
| $^{58}$Ni | 68.000 | 0.009 | $^{58}$Ni(n,2n)$^{57}$Ni | 128160 | 216 | 1377.63 | 0.03 | 0.817 | 0.024 |
| $^{58}$Ni | 68.000 | 0.009 | $^{58}$Ni(n,2n)$^{57}$Ni | 128160 | 216 | 1757.55 | 0.03 | 0.0575 | 0.002 |
| $^{58}$Ni | 68.000 | 0.009 | $^{58}$Ni(n,2n)$^{57}$Ni | 128160 | 216 | 1919.52 | 0.05 | 0.123 | 0.004 |
| $^{58}$Ni | 68.000 | 0.008 | $^{58}$Ni(n,d or np)$^{57}$Co | 23478336 | 12096 | 122.0607 | 0.00012 | 0.856 | 0.0017 |
| $^{58}$Ni | 68.000 | 0.008 | $^{58}$Ni(n,d or np)$^{57}$Co | 23478336 | 12096 | 136.4736 | 0.00029 | 0.1068 | 0.0008 |
| $^{35}$Cl | 75.760 | 0.100 | $^{35}$Cl(n,2n)$^{34m}$Cl | 1920 | 2.4 | 146.36 | 0.03 | 0.383 | 0.005 |
| $^{37}$Cl | 24.240 | 0.100 | $^{37}$Cl(n,p)$^{37}$S | 303 | 120 | 3103.37 | 0.02 | 0.939 | - |
| $^{51}$V | 99.750 | 0.002 | $^{51}$V(n,p)$^{51}$Ti | 345.6 | 0.6 | 320.076 | 0.006 | 0.931 | - |
| $^{51}$V | 99.750 | 0.002 | $^{51}$V(n,a)$^{48}$Sc | 157212 | 324 | 983.526 | 0.012 | 1.001 | 0.006 |
| $^{51}$V | 99.750 | 0.002 | $^{51}$V(n,a)$^{48}$Sc | 157212 | 324 | 1312.12 | 0.012 | 1.001 | 0.007 |
| $^{51}$V | 99.750 | 0.002 | $^{51}$V(n,a)$^{48}$Sc | 157212 | 324 | 1037.522 | 0.012 | 0.976 | 0.007 |
| $^{64}$Zn | 49.170 | 0.750 | $^{64}$Zn(n,2n)$^{63}$Zn | 2308.2 | 3 | 669.62 | 0.05 | 0.082 | - |
| $^{70}$Zn | 0.610 | 0.100 | $^{70}$Zn(n,2n)$^{69m}$Zn | 49521.6 | 64.8 | 438.634 | 0.018 | 0.9485 | 0.0007 |
| $^{24}$Mg | 78.990 | 0.040 | $^{24}$Mg(n,p)$^{24}$Na | 53989.2 | 43.2 | 1368.626 | 0.005 | 0.999936 | 0.000015 |
| $^{24}$Mg | 78.990 | 0.040 | $^{24}$Mg(n,p)$^{24}$Na | 53989.2 | 43.2 | 2754.007 | 0.011 | 0.99855 | 0.00005 |
| $^{90}$Zr | 51.450 | 0.400 | $^{90}$Zr(n,2n)$^{89}$Zr | 282276 | 432 | 909.15 | 0.15 | 0.9904 | - |
| $^{90}$Zr | 51.450 | 0.400 | $^{90}$Zr(n,p)$^{90m}$Y | 11484 | 216 | 479.51 | 0.05 | 0.9074 | 0.004 |
| $^{90}$Zr | 51.450 | 0.400 | $^{90}$Zr(n,p)$^{90m}$Y | 11484 | 216 | 202.53 | 0.03 | 0.973 | 0.004 |
| $^{93}$Nb | 100.000 | 0.000 | $^{93}$Nb(n,2n)$^{92m}$Nb | 876960 | 1728 | 934.44 | 0.1 | 0.9915 | - |
| $^{93}$Nb | 100.000 | 0.000 | $^{93}$Nb(n,a)$^{90m}$Y | 11484 | 216 | 202.53 | 0.03 | 0.973 | 0.004 |
| $^{93}$Nb | 100.000 | 0.000 | $^{93}$Nb(n,a)$^{90m}$Y | 11484 | 216 | 479.51 | 0.05 | 0.9074 | 0.0005 |

Table 2. Specifications of the foils in the kit.

| Element | Set #1 (60 μA−90 kV high-yield) | | Set #2 (30 μA−70 kV low-yield) | | Diameter [inch] | Density [g/cm$^3$] |
|---|---|---|---|---|---|---|
| | Thickness [cm] | Sample mass [g] | Thickness [cm] | Sample mass [g] | | |
| Al | 0.0127 | 0.0406 | 0.0127 | 0.0415 | 0.5 | 2.70 |
| Cu | 0.0127 | 0.1406 | 0.0127 | 0.1436 | 0.5 | 8.96 |
| Fe | 0.0127 | 0.1349 | 0.0127 | 0.1335 | 0.5 | 7.87 |
| Ti | 0.0254 | 0.1447 | 0.0254 | 0.1423 | 0.5 | 4.54 |
| In | 0.0127 | 0.1167 | 0.0127 | 0.1082 | 0.5 | 7.31 |

| | | | | | | |
|---|---|---|---|---|---|---|
| Ni | 0.0254 | 0.2818 | 0.0254 | 0.2812 | 0.5 | 8.90 |
| Na + Cl | 0.1905 | 0.4877 | 0.1905 | 0.4806 | 0.5 | 2.16 |
| V | 0.0051 | 0.0433 | 0.0051 | 0.0423 | 0.5 | 6.11 |
| Zn | 0.0254 | 0.2324 | 0.0254 | 0.2319 | 0.5 | 7.13 |
| Mg | 0.0127 | 0.0286 | 0.0127 | 0.0285 | 0.5 | 1.74 |
| Zr | 0.0127 | 0.1116 | 0.0127 | 0.1112 | 0.5 | 6.51 |
| Nb | 0.0254 | 0.2740 | 0.0254 | 0.2728 | 0.5 | 8.57 |

Table 3. Summary of Irradiation, real and live counting and delay times.

| Foil | Set #1 (60 μA−90 kV high-yield) | | | | Set #2 (30 μA−70 kV low-yield) | | | |
|---|---|---|---|---|---|---|---|---|
| | $t_{irr}$ [s] | $t_c$ [s] | $t_{live}$ [s] | $t_d$ [s] | $t_{irr}$ [s] | $t_c$ [s] | $t_{live}$ [s] | $t_d$ [s] |
| Al | 21600 | 43590 | 43200 | 36 | 21600 | 43592 | 43200 | 36 |
| Cu | 21600 | 43577 | 43200 | 36 | 21600 | 43571 | 43200 | 39 |
| Fe | 21600 | 43587 | 43200 | 40 | 21600 | 43588 | 43200 | 40 |
| Ti | 28800 | 87165 | 86400 | 40 | 28800 | 87174 | 86400 | 36 |
| In | 28800 | 87156 | 86400 | 45 | 28800 | 87207 | 86400 | 42 |
| Ni | 28800 | 87196 | 86400 | 40 | 28800 | 87147 | 86400 | 38 |
| Na+Cl | 21600 | 43604 | 43200 | 37 | 21600 | 43608 | 43200 | 38 |
| V | 28800 | 87163 | 86400 | 43 | 28800 | 87219 | 86400 | 35 |
| Zn | 21600 | 43589 | 43200 | 44 | 21600 | 43577 | 43200 | 44 |
| Mg | 21600 | 43584 | 43200 | 40 | 21600 | 43586 | 43200 | 14 |
| Zr | 28800 | 87243 | 86400 | 35 | 28800 | 87190 | 86400 | 40 |
| Nb | 28800 | 87191 | 86400 | 59 | 28800 | 87165 | 86400 | 40 |

Table 4. Summary of the measurements to derive an absolute full energy peak efficiency function.

| Radioisotope | $E_i$ [keV] | $T_{1/2}$ [days] | $r_i$ (calibrated as of 1/1/18) | $R(E_i)$ | $N(E_i)$ | $N(E_i)/R(E_i)$ |
|---|---|---|---|---|---|---|
| $^{241}$Am | 59.5 | 1.580E+05 | 1.250E+03 | 2.907E+07 | 4.169E+06 | 1.434E-01 |
| $^{109}$Cd | 88 | 4.614E+02 | 6.010E+02 | 1.334E+07 | 2.459E+06 | 1.843E-01 |
| $^{57}$Co | 122.1 | 2.717E+02 | 5.060E+02 | 1.087E+07 | 2.172E+06 | 1.998E-01 |
| $^{139}$Ce | 165.9 | 1.376E+02 | 5.850E+02 | 1.163E+07 | 1.968E+06 | 1.692E-01 |
| $^{203}$Hg | 279 | 4.661E+01 | 1.190E+03 | 1.742E+07 | 2.009E+06 | 1.154E-01 |
| $^{113}$Sn | 391.7 | 1.151E+02 | 1.620E+03 | 3.124E+07 | 2.644E+06 | 8.465E-02 |

| | | | | | | |
|---|---|---|---|---|---|---|
| $^{137}$Cs | 661.7 | 1.099E+04 | 2.430E+03 | 5.642E+07 | 2.954E+06 | 5.235E-02 |
| $^{88}$Y | 898 | 1.066E+02 | 5.080E+03 | 9.650E+07 | 3.323E+06 | 3.444E-02 |
| $^{60}$Co | 1173.2 | 1.925E+03 | 3.350E+03 | 7.706E+07 | 2.062E+06 | 2.675E-02 |
| $^{60}$Co | 1332.5 | 1.925E+03 | 3.360E+03 | 7.729E+07 | 1.814E+06 | 2.346E-02 |
| $^{88}$Y | 1836.1 | 1.066E+02 | 5.370E+03 | 1.020E+08 | 1.798E+06 | 1.763E-02 |
| $t_c$ | 28123 s | | | | | |
| $t_{live}$ | 23263 s | | | | | |
| $\Delta t$ | 31 days (efficiency measurements were done on 2/1/2018) | | | | | |
| $a_0$ | -25.43710 | | | | | |
| $a_1$ | 12.79550 | | | | | |
| $a_2$ | -2.22297 | | | | | |
| $a_3$ | 0.12811 | | | | | |
| $a_4$ | -0.00112 | | | | | |

Table 5. Summary of net count ($N_i$) from peak analysis and calculated coefficient ($C_i$) for each gamma-ray peak. Some gamma-ray peaks in the set #2 were not analyzed due to low counting statistics, and these peaks were not taken into account in determination of the neutron flux. $m$ = 41 for the set #1 and $m$ = 35 for the set #2 in Equation ((2).

| Reaction | $E_\gamma$ [keV] | Set #1 (60 μA−90 kV high-yield) | | Set #2 (30 μA−70 kV low-yield) | |
|---|---|---|---|---|---|
| | | $N_i$ | $C_i$ | $N_i$ | $C_i$ |
| $^{27}$Al(n,p)$^{27}$Mg | 843.76 | 936 | 1.909E+22 | 166 | 1.951E+22 |
| | 1014.52 | 214 | 6.107E+21 | | |
| $^{27}$Al(n,α)$^{24}$Na | 1368.63 | 14978 | 1.661E+23 | 1465 | 1.698E+23 |
| | 2754.01 | 7203 | 9.640E+22 | 665 | 9.854E+22 |
| $^{65}$Cu(n,2n)$^{64}$Cu | 511.00 | 10051 | 2.190E+22 | 915 | 2.237E+22 |
| | 1345.77 | 150 | 4.000E+20 | | |

| | | | | | |
|---|---|---|---|---|---|
| $^{56}Fe(n,p)^{56}Mn$ | 846.76 | 35424 | 5.050E+23 | 4198 | 4.997E+23 |
| | 1810.73 | 4170 | 6.500E+22 | 452 | 6.433E+22 |
| | 2113.09 | 1854 | 3.041E+22 | 148 | 3.010E+22 |
| $^{47}Ti(n,p)^{47}Sc$ | 159.38 | 9522 | 8.246E+22 | 881 | 8.109E+22 |
| $^{48}Ti(n,p)^{48}Sc$ | 983.53 | 10688 | 3.673E+23 | 698 | 3.612E+23 |
| | 1037.52 | 9259 | 3.384E+23 | 932 | 3.328E+23 |
| | 175.36 | 3148 | 1.236E+23 | 885 | 1.216E+23 |
| | 1312.12 | 7734 | 2.734E+23 | 785 | 2.689E+23 |
| $^{115}In(n,2n)^{114m}In$ | 558.43 | 577 | 6.102E+20 | 449 | 5.657E+20 |
| | 190.27 | 4876 | 5.656E+21 | 3283 | 5.244E+21 |
| $^{115}In(n,n')^{115m}In$ | 336.24 | 29145 | 4.283E+23 | 4412 | 3.970E+23 |
| $^{115}In(n,\gamma)^{116m}In$ | 1293.56 | 1337 | 5.524E+22 | 216 | 5.123E+22 |
| | 1097.28 | 934 | 4.502E+22 | 152 | 4.175E+22 |
| $^{58}Ni(n,p)^{58}Co$ | 810.76 | 4604 | 2.148E+22 | 3977 | 2.144E+22 |
| $^{58}Ni(n,2n)^{57}Ni$ | 1377.63 | 4280 | 3.611E+23 | | |
| | 1757.55 | 152 | 2.040E+22 | | |
| | 1919.52 | 795 | 4.060E+22 | 22 | 4.052E+22 |
| $^{58}Ni(n,d)+(n,np)^{57}Co$ | 122.06 | 9580 | 2.254E+22 | 9342 | 2.249E+22 |
| | 136.47 | 1344 | 2.750E+21 | 3115 | 2.744E+21 |
| $^{35}Cl(n,2n)^{34m}Cl$ | 146.36 | 1890 | 6.875E+23 | 54 | 6.770E+23 |
| $^{37}Cl(n,p)^{37}S$ | 3103.37 | 65 | 5.672E+21 | 8 | 5.572E+21 |
| $^{51}V(n,p)^{51}Ti$ | 320.08 | 443 | 2.259E+22 | | |
| $^{51}V(n,\alpha)^{48}Sc$ | 983.53 | 1062 | 1.401E+23 | 101 | 1.368E+23 |
| | 1312.12 | 584 | 1.042E+23 | 189 | 1.018E+23 |
| | 1037.52 | 715 | 1.291E+23 | 45 | 1.261E+23 |
| $^{64}Zn(n,2n)^{63}Zn$ | 669.62 | 717 | 1.360E+22 | | |
| $^{70}Zn(n,2n)^{69m}Zn$ | 438.63 | 3169 | 7.977E+21 | 620 | 7.960E+21 |
| $^{24}Mg(n,p)^{24}Na$ | 1368.63 | 5686 | 1.026E+23 | 1234 | 1.023E+23 |
| | 2754.01 | 2862 | 5.956E+22 | 701 | 5.937E+22 |
| $^{90}Zr(n,2n)^{89}Zr$ | 909.15 | 31177 | 6.937E+22 | 6252 | 6.913E+22 |
| $^{90}Zr(n,p)^{90m}Y$ | 479.51 | 1979 | 3.011E+23 | 535 | 3.215E+23 |
| | 202.53 | 4936 | 7.437E+23 | 254 | 7.413E+23 |
| $^{93}Nb(n,2n)^{92m}Nb$ | 934.44 | 38745 | 1.114E+23 | 8132 | 1.109E+23 |
| $^{93}Nb(n,\alpha)^{90m}Y$ | 202.53 | 8980 | 3.427E+24 | 1382 | 3.417E+24 |
| | 479.51 | 3993 | 1.501E+24 | 970 | 1.496E+24 |

Table 6. Neutron induced reaction cross-sections from 1 to 15 MeV. *n* is equal to 15 in Equation ((2) where *m* is required to be larger than *n*. Cross-sections are presented in the unit of barns [$10^{-24}$ $cm^2$].

| Reaction | Neutron energy [MeV] | | | | | | | | | | | | | | |
|---|---|---|---|---|---|---|---|---|---|---|---|---|---|---|---|
| | 1.0 | 2.0 | 3.0 | 4.0 | 5.0 | 6.0 | 7.0 | 8.0 | 9.0 | 10.0 | 11.0 | 12.0 | 13.0 | 14.0 | 15.0 |
| $^{27}Al(n,p)^{27}Mg$ | 0.00E+00 | 8.69E-08 | 1.08E-03 | 6.03E-03 | 1.93E-02 | 4.70E-02 | 5.69E-02 | 7.41E-02 | 8.15E-02 | 9.11E-02 | 8.81E-02 | 8.46E-02 | 8.11E-02 | 7.31E-02 | 6.52E-02 |
| $^{27}Al(n,a)^{24}Na$ | 0.00E+00 | 0.00E+00 | 0.00E+00 | 3.78E-13 | 1.34E-05 | 1.39E-03 | 1.72E-02 | 4.10E-02 | 7.14E-02 | 8.92E-02 | 1.07E-01 | 1.18E-01 | 1.25E-01 | 1.23E-01 | 1.09E-01 |
| $^{65}Cu(n,2n)^{64}Cu$ | 0.00E+00 | 0.00E+00 | 0.00E+00 | 0.00E+00 | 0.00E+00 | 0.00E+00 | 0.00E+00 | 0.00E+00 | 0.00E+00 | 0.00E+00 | 1.22E-01 | 4.13E-01 | 6.65E-01 | 8.37E-01 | 9.39E-01 |
| $^{56}Fe(n,p)^{56}Mn$ | 0.00E+00 | 0.00E+00 | 3.46E-11 | 5.24E-06 | 9.98E-04 | 1.34E-02 | 3.04E-02 | 4.62E-02 | 6.07E-02 | 7.30E-02 | 8.77E-02 | 1.04E-01 | 1.15E-01 | 1.14E-01 | 1.03E-01 |
| $^{47}Ti(n,p)^{47}Sc$ | 4.10E-04 | 9.69E-03 | 3.13E-02 | 5.61E-02 | 8.30E-02 | 1.05E-01 | 1.21E-01 | 1.32E-01 | 1.37E-01 | 1.42E-01 | 1.46E-01 | 1.48E-01 | 1.51E-01 | 1.46E-01 | 1.34E-01 |
| $^{48}Ti(n,p)^{48}Sc$ | 0.00E+00 | 0.00E+00 | 0.00E+00 | 1.61E-08 | 1.04E-04 | 2.07E-03 | 8.33E-03 | 1.70E-02 | 2.66E-02 | 3.55E-02 | 4.31E-02 | 4.95E-02 | 5.34E-02 | 5.90E-02 | 6.18E-02 |

| | | | | | | | | | | | | | | | |
|---|---|---|---|---|---|---|---|---|---|---|---|---|---|---|---|
| $^{115}In(n,2n)^{114m}In$ | 0.00E+00 | 0.00E+00 | 0.00E+00 | 0.00E+00 | 0.00E+00 | 0.00E+00 | 0.00E+00 | 0.00E+00 | 0.00E+00 | 1.38E-01 | 5.70E-01 | 9.51E-01 | 1.19E+00 | 1.33E+00 | 1.39E+00 |
| $^{115}In(n,n')^{115m}In$ | 6.82E-02 | 2.68E-01 | 3.41E-01 | 3.21E-01 | 3.29E-01 | 3.49E-01 | 3.29E-01 | 3.12E-01 | 2.91E-01 | 2.61E-01 | 2.05E-01 | 1.49E-01 | 9.31E-02 | 6.25E-02 | 5.80E-02 |
| $^{115}In(n,\gamma)^{116m}In$ | 1.83E-01 | 1.24E-01 | 5.44E-02 | 2.46E-02 | 1.32E-02 | 6.29E-03 | 3.34E-03 | 2.23E-03 | 1.56E-03 | 1.14E-03 | 1.00E-03 | 8.96E-04 | 9.32E-04 | 9.68E-04 | 1.00E-03 |
| $^{58}Ni(n,p)^{58}Co$ | 7.98E-04 | 3.80E-02 | 1.86E-01 | 3.63E-01 | 5.10E-01 | 5.94E-01 | 6.23E-01 | 6.30E-01 | 6.36E-01 | 6.30E-01 | 6.07E-01 | 5.66E-01 | 4.74E-01 | 3.54E-01 | 2.50E-01 |
| $^{58}Ni(n,2n)^{57}Ni$ | 0.00E+00 | 0.00E+00 | 0.00E+00 | 0.00E+00 | 0.00E+00 | 0.00E+00 | 0.00E+00 | 0.00E+00 | 0.00E+00 | 0.00E+00 | 0.00E+00 | 0.00E+00 | 3.81E-03 | 2.27E-02 | 4.25E-02 |
| $^{58}Ni(n,d\ or\ np)^{57}Co$ | 0.00E+00 | 0.00E+00 | 0.00E+00 | 0.00E+00 | 0.00E+00 | 0.00E+00 | 1.76E-10 | 4.19E-06 | 1.46E-04 | 6.14E-03 | 8.13E-02 | 2.37E-01 | 4.19E-01 | 5.69E-01 | 6.82E-01 |
| $^{35}Cl(n,2n)^{34m}Cl$ | 0.00E+00 | 0.00E+00 | 0.00E+00 | 0.00E+00 | 0.00E+00 | 0.00E+00 | 0.00E+00 | 0.00E+00 | 0.00E+00 | 0.00E+00 | 0.00E+00 | 0.00E+00 | 0.00E+00 | 4.04E-03 | 1.15E-02 |
| $^{37}Cl(n,p)^{37}S$ | 0.00E+00 | 0.00E+00 | 0.00E+00 | 0.00E+00 | 2.69E-04 | 6.03E-04 | 4.59E-03 | 9.72E-03 | 1.31E-02 | 1.85E-02 | 2.29E-02 | 2.44E-02 | 2.42E-02 | 2.40E-02 | 2.10E-02 |
| $^{51}V(n,p)^{51}Ti$ | 0.00E+00 | 3.34E-14 | 3.86E-05 | 1.03E-03 | 3.00E-03 | 5.64E-03 | 9.06E-03 | 1.30E-02 | 1.72E-02 | 2.15E-02 | 2.54E-02 | 2.84E-02 | 3.06E-02 | 3.10E-02 | 3.01E-02 |
| $^{51}V(n,a)^{48}Sc$ | 0.00E+00 | 0.00E+00 | 1.80E-18 | 4.19E-13 | 1.04E-08 | 3.48E-06 | 9.69E-05 | 8.47E-04 | 2.92E-03 | 5.37E-03 | 7.57E-03 | 9.99E-03 | 1.27E-02 | 1.49E-02 | 1.75E-02 |
| $^{64}Zn(n,2n)^{63}Zn$ | 0.00E+00 | 0.00E+00 | 0.00E+00 | 0.00E+00 | 0.00E+00 | 0.00E+00 | 0.00E+00 | 0.00E+00 | 0.00E+00 | 0.00E+00 | 0.00E+00 | 0.00E+00 | 2.98E-02 | 1.07E-01 | 1.83E-01 |
| $^{70}Zn(n,2n)^{69m}Zn$ | 0.00E+00 | 0.00E+00 | 0.00E+00 | 0.00E+00 | 0.00E+00 | 0.00E+00 | 0.00E+00 | 0.00E+00 | 0.00E+00 | 2.50E-02 | 2.72E-01 | 4.82E-01 | 6.06E-01 | 6.76E-01 | 7.26E-01 |
| $^{24}Mg(n,p)^{24}Na$ | 0.00E+00 | 0.00E+00 | 0.00E+00 | 0.00E+00 | 2.10E-05 | 3.50E-03 | 4.40E-02 | 1.13E-01 | 1.21E-01 | 1.48E-01 | 1.70E-01 | 1.90E-01 | 1.98E-01 | 1.97E-01 | 1.78E-01 |
| $^{90}Zr(n,2n)^{89}Zr$ | 0.00E+00 | 0.00E+00 | 0.00E+00 | 0.00E+00 | 0.00E+00 | 0.00E+00 | 0.00E+00 | 0.00E+00 | 0.00E+00 | 0.00E+00 | 0.00E+00 | 0.00E+00 | 2.28E-01 | 5.18E-01 | 7.22E-01 |
| $^{90}Zr(n,p)^{90m}Y$ | 0.00E+00 | 0.00E+00 | 2.74E-07 | 6.21E-07 | 1.93E-05 | 2.42E-04 | 8.30E-04 | 1.86E-03 | 3.26E-03 | 4.87E-03 | 6.71E-03 | 8.66E-03 | 1.06E-02 | 1.20E-02 | 1.27E-02 |
| $^{93}Nb(n,2n)^{92m}Nb$ | 0.00E+00 | 0.00E+00 | 0.00E+00 | 0.00E+00 | 0.00E+00 | 0.00E+00 | 0.00E+00 | 0.00E+00 | 0.00E+00 | 1.27E-01 | 2.85E-01 | 3.90E-01 | 4.42E-01 | 4.59E-01 | 4.60E-01 |
| $^{93}Nb(n,a)^{90m}Y$ | 2.33E-07 | 1.44E-06 | 9.06E-06 | 3.90E-05 | 1.27E-04 | 3.23E-04 | 6.56E-04 | 1.17E-03 | 1.74E-03 | 2.46E-03 | 3.30E-03 | 4.17E-03 | 4.98E-03 | 5.60E-03 | 5.80E-03 |

Table 7. Summary of neutron yields. Neutron yields are given in the unit of n/s.

| | Remetti et al. (2017) | | | Alexa and Uhlář (2013) | | | PINS (2018) | |
|---|---|---|---|---|---|---|---|---|
| *V* \ *I* | 20 μA | 40 μA | 60 μA | 20 μA | 40 μA | 60 μA | 30 μA | 60 μA |
| 40 kV | 2.70E+06 | 5.73E+06 | 8.64E+06 | 0.00E+00 | 0.00E+00 | 0.00E+00 | | |
| 50 kV | 6.94E+06 | 1.33E+07 | 2.00E+07 | 4.19E+06 | 8.65E+06 | 1.31E+07 | | |
| 60 kV | 1.28E+07 | 2.74E+07 | 4.12E+07 | 1.17E+07 | 2.43E+07 | 3.69E+07 | | |
| 70 kV | 2.15E+07 | 4.76E+07 | 7.15E+07 | 2.12E+07 | 4.44E+07 | 6.76E+07 | 2.28E+07 | |
| 80 kV | 3.42E+07 | 7.33E+07 | 1.10E+08 | 3.21E+07 | 6.79E+07 | 1.04E+08 | | |
| 90 kV | 5.20E+07 | 1.04E+08 | 1.56E+08 | 4.43E+07 | 9.42E+07 | 1.44E+08 | | 1.73E+08 |
| 100 kV | 7.61E+07 | 1.39E+08 | 2.08E+08 | 5.74E+07 | 1.23E+08 | 1.89E+08 | | |

Table 8. Average of ten 30-second dose rate readings for each generator setting. Dose rates are given in the unit of mrem/hr.

| *V* \ *I* | 60 μA | 55uA | 50uA | 45uA | 40uA | 35uA | 30uA | 25 μA |
|---|---|---|---|---|---|---|---|---|
| 90 kV | 155.5 | 141.2 | 122.8 | 101.1 | 66.6 | 41.5 | 29.6 | 21.6 |
| 85 kV | 128.2 | 117.3 | 104.6 | 88.6 | 64.2 | 39.8 | 25.9 | 19.0 |
| 80 kV | 104.0 | 93.8 | 85.2 | 74.9 | 57.9 | 38.7 | 25.9 | 16.0 |
| 75 kV | 83.5 | 77.0 | 69.2 | 61.4 | 49.1 | 36.5 | 21.1 | 13.0 |
| 70 kV | 64.6 | 60.1 | 53.8 | 48.3 | 40.9 | 31.9 | 19.9 | 11.0 |
| 65 kV | 49.4 | 45.6 | 41.2 | 36.5 | 31.9 | 26.1 | 18.3 | 9.9 |
| 60 kV | 35.7 | 33.3 | 30.1 | 27.0 | 23.7 | 20.3 | 15.2 | 9.1 |
| 55 kV | 25.5 | 23.6 | 21.3 | 19.1 | 16.8 | 14.4 | 11.7 | 7.8 |
| 50 kV | 17.2 | 16.0 | 14.4 | 13.1 | 11.4 | 9.8 | 8.4 | 6.1 |
| 45 kV | 11.0 | 10.0 | 9.4 | 8.5 | 7.4 | 6.5 | 5.4 | 4.4 |
| 40 kV | 6.4 | 6.1 | 5.6 | 5.0 | 4.4 | 3.9 | 3.3 | 2.7 |


Figure 1. The Foils included in the kit from Shieldwerx™. The kit comes with two foils of Al, Cu, Fe, Mg, NaCl, Nb, Ni, Ti, V, Zn and Zr each. Sulfur foils were not used in this study due to the lack of gamma-rays. Each foil's thickness and mass were measured and labelled by the manufacturer. The first set of 12 foils was activated by the generator operated at 30 μA−70 kV while the second set of the remaining 12 foils was irradiated at 60 μA−90 kV.

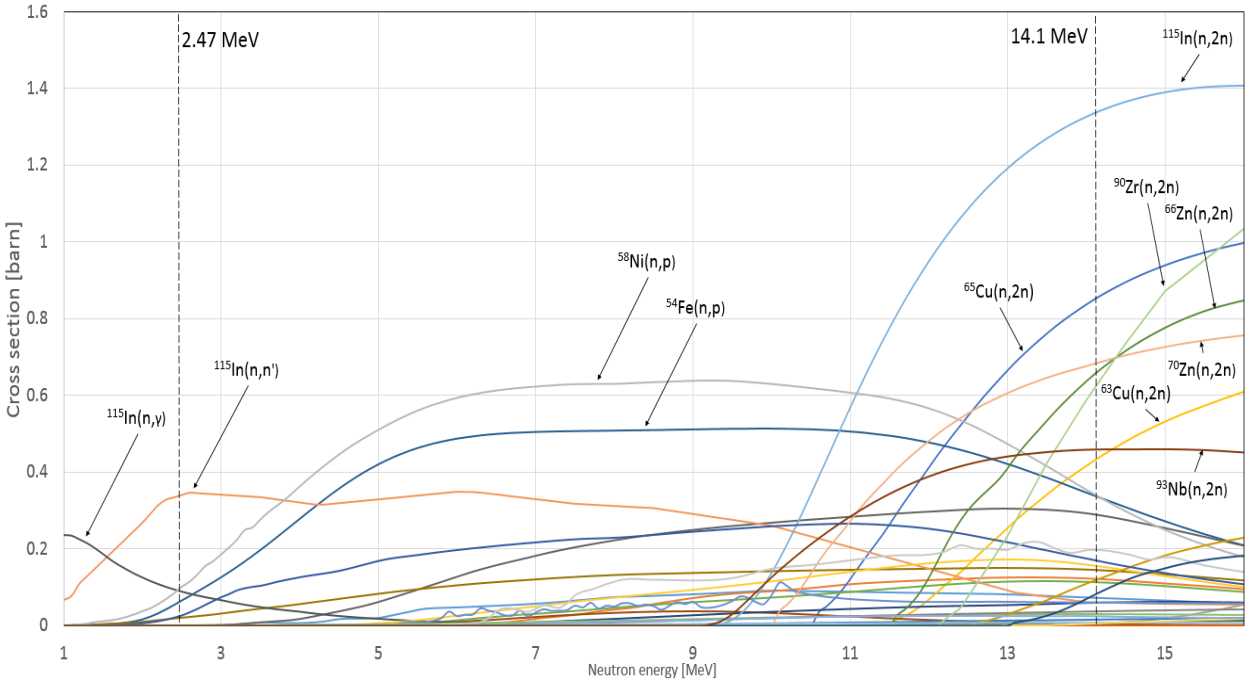


Figure 2. Neutron induced reaction cross sections for the isotopes included in the foil kit.

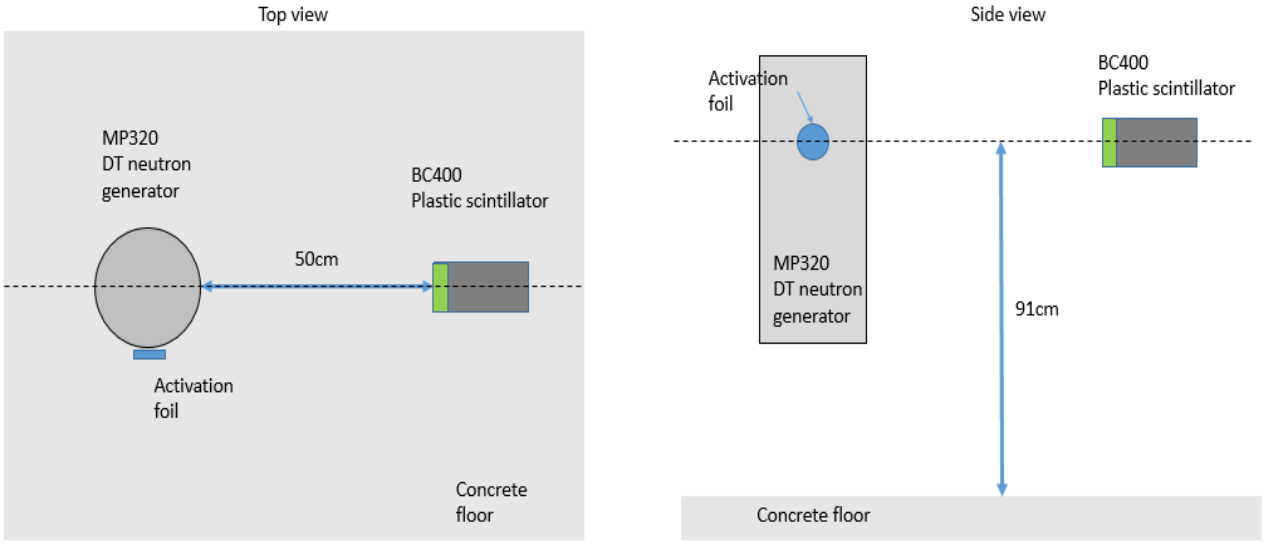


Figure 3. Schematic diagrams of the experimental setup in the PINS lab (not drawn to scale)

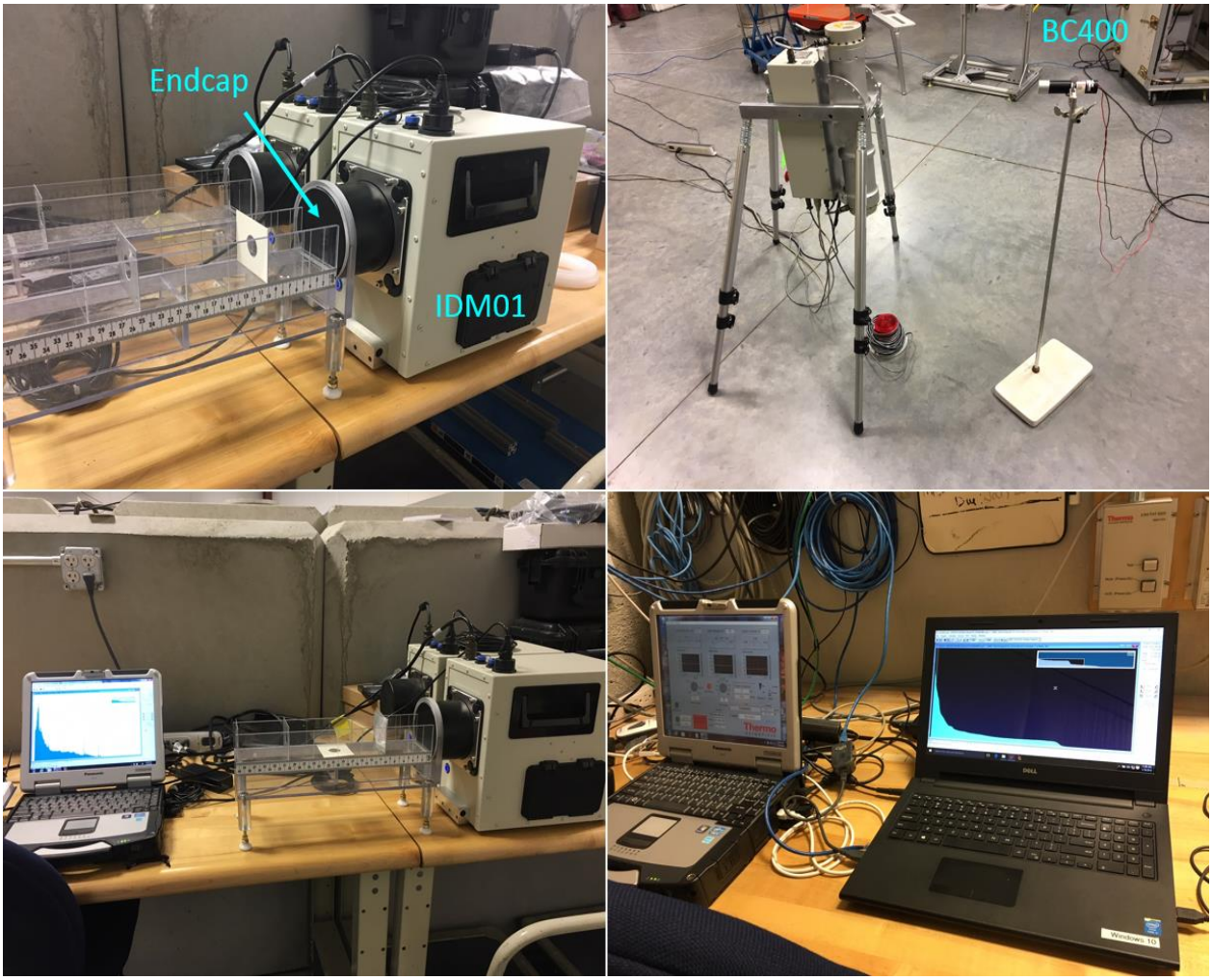


Figure 4. Experimental setups in the PINS lab. (Top left) two ORTEC® HPGe detectors (IDM01 and IDM02) at the counting station. (Top right) an MP320 generator and a BC400 scintillator. (Bottom left) the IDM01 is being used to collect data from a calibration source. (Bottom right) a typical BC400 spectrum while a neutron generator is turned on.

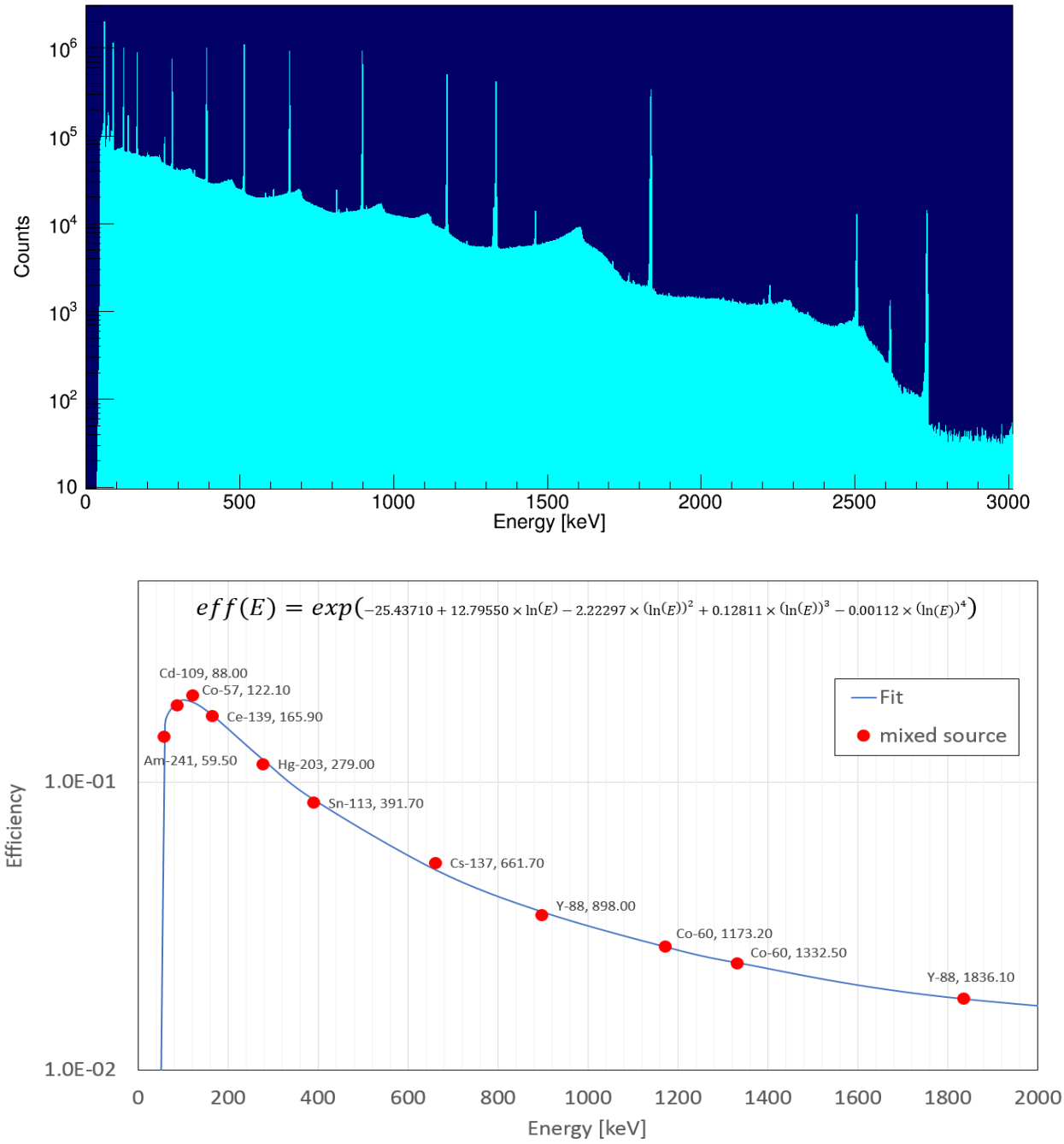


Figure 5. (Top) the IDM01's gamma-ray spectrum with a mixed radiation source collected for 28123 seconds. (Bottom) the IDM01's absolute full energy peak efficiency at the endcap position is plotted with the 11 discrete data points from the measurements. 11 out of 12 characteristic gamma-rays were used for this analysis.

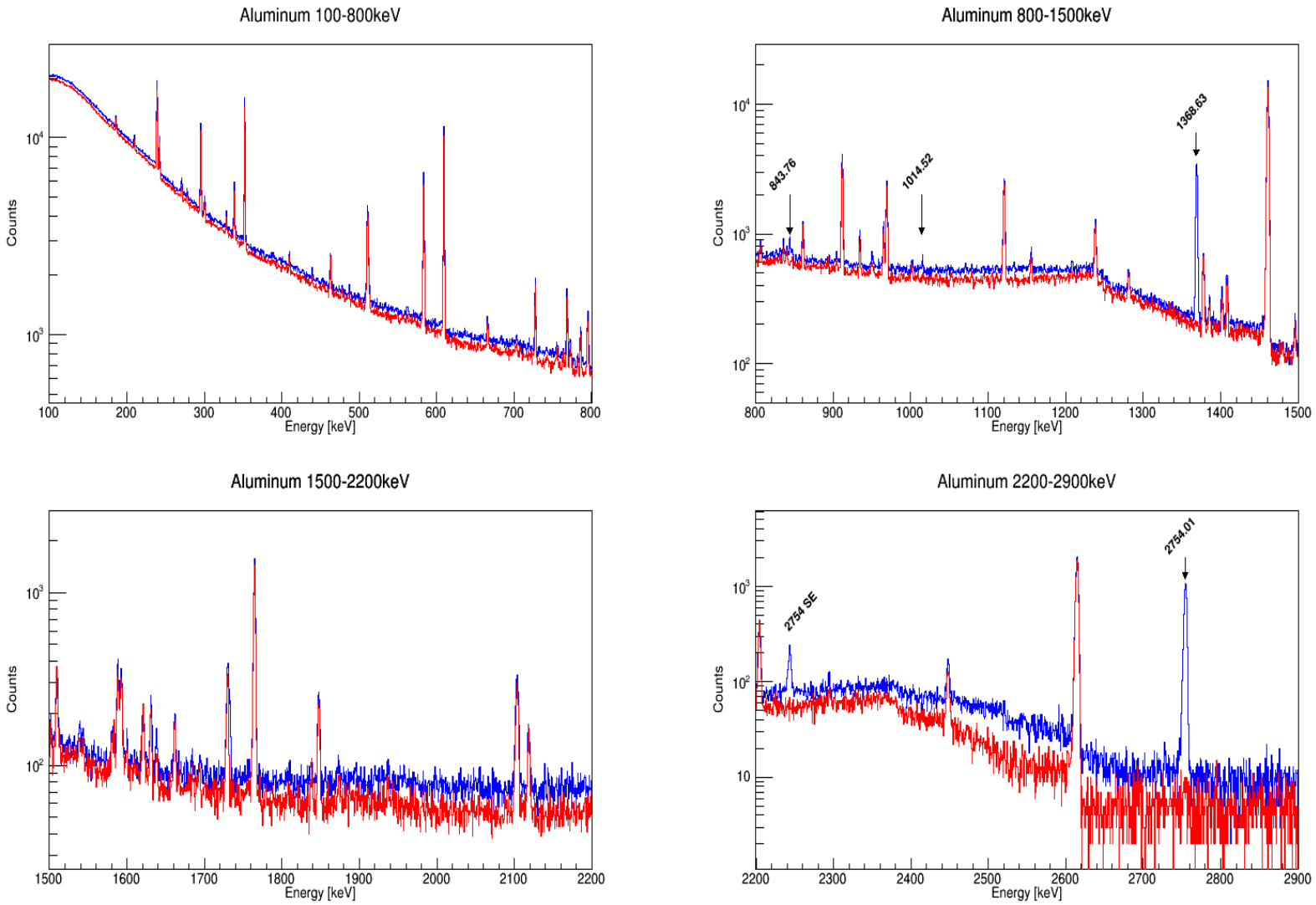


Figure 6. Aluminum spectrum (blue) was collected for 12 hours, and the 12-hour background spectrum (red) is also shown for comparison.

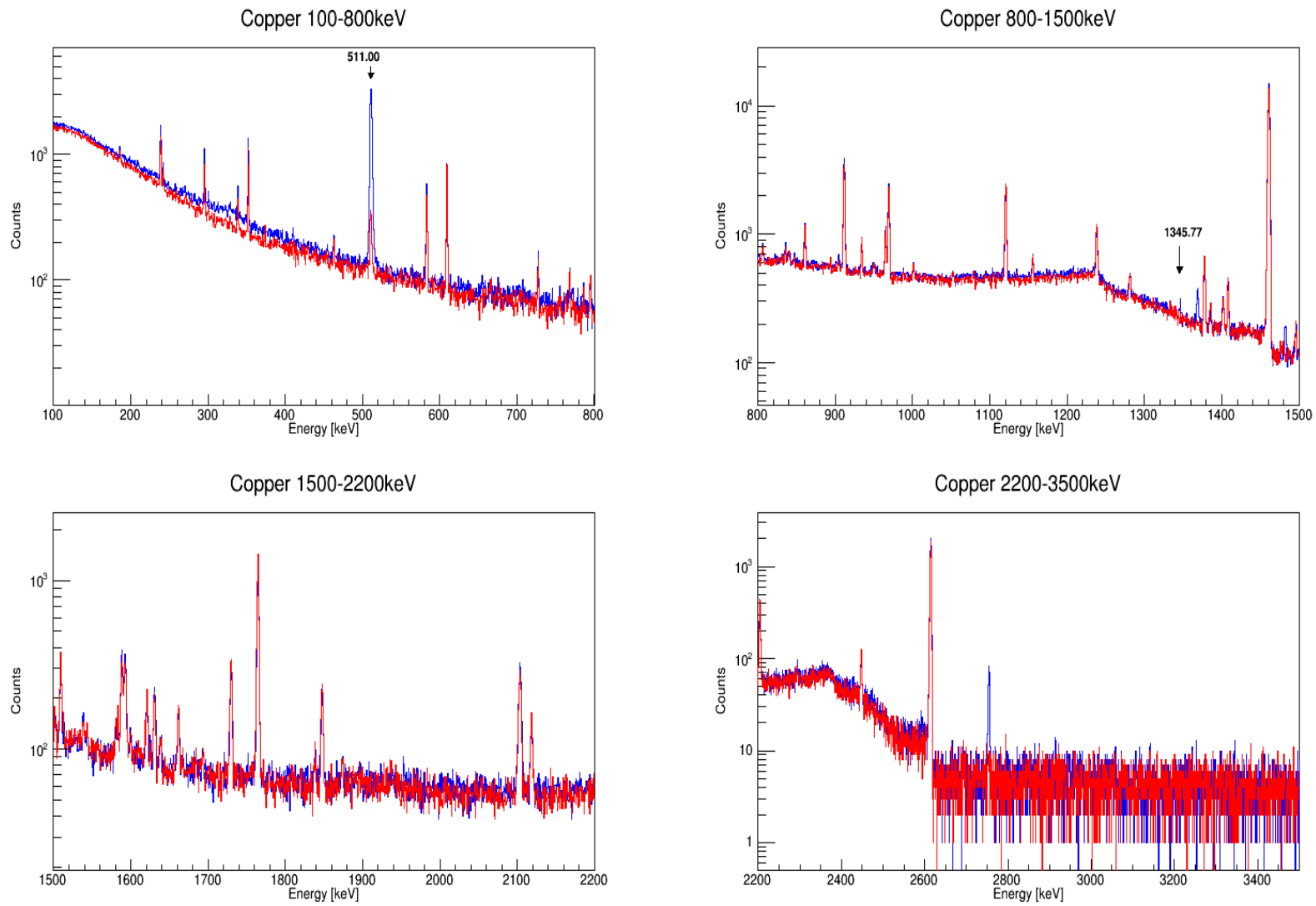


Figure 7. Copper spectrum (blue) was collected for 12 hours, and the 12-hour background spectrum (red) is also shown for comparison.

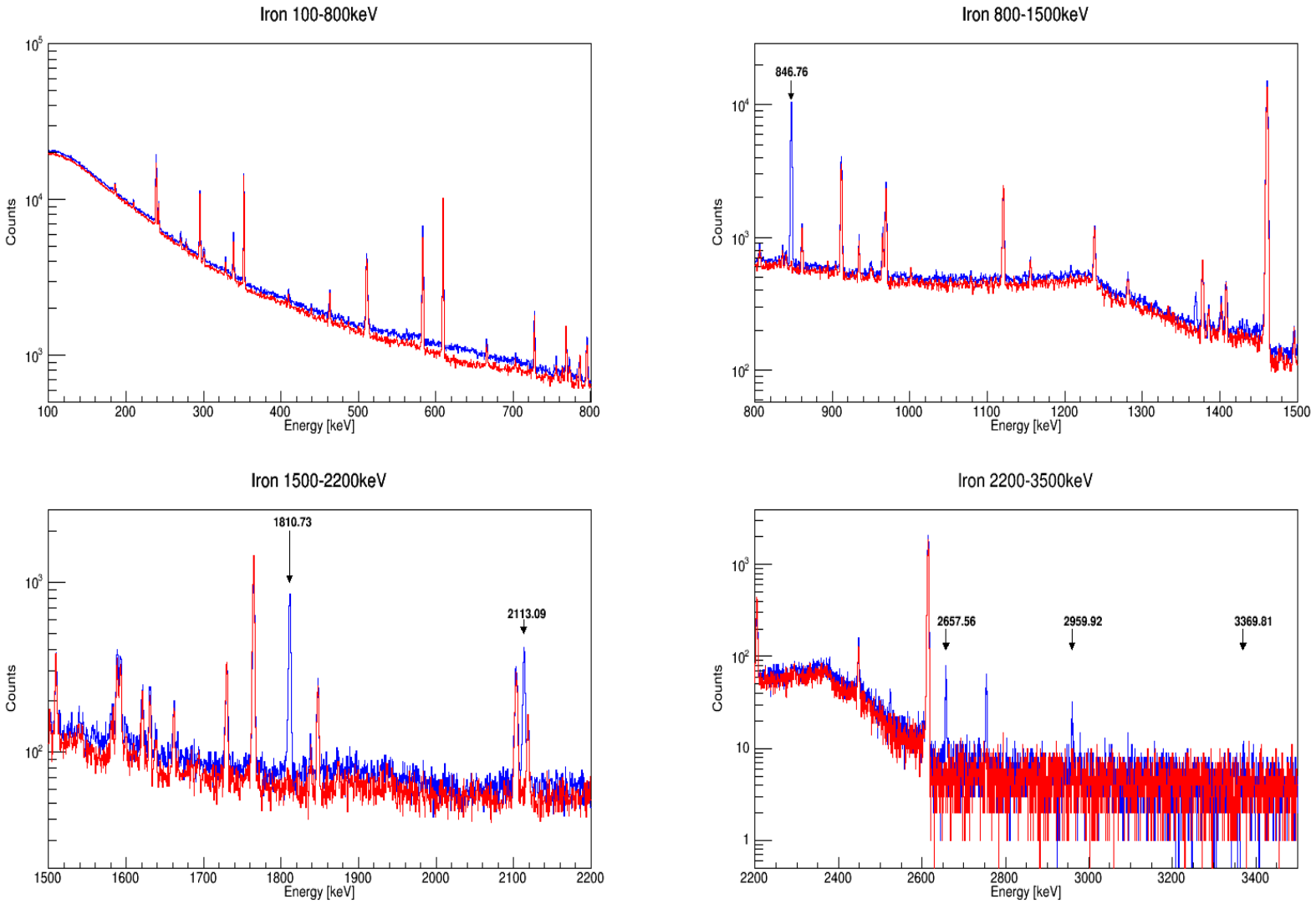


Figure 8. Iron spectrum (blue) was collected for 12 hours, and the 12-hour background spectrum (red) is also shown for comparison.

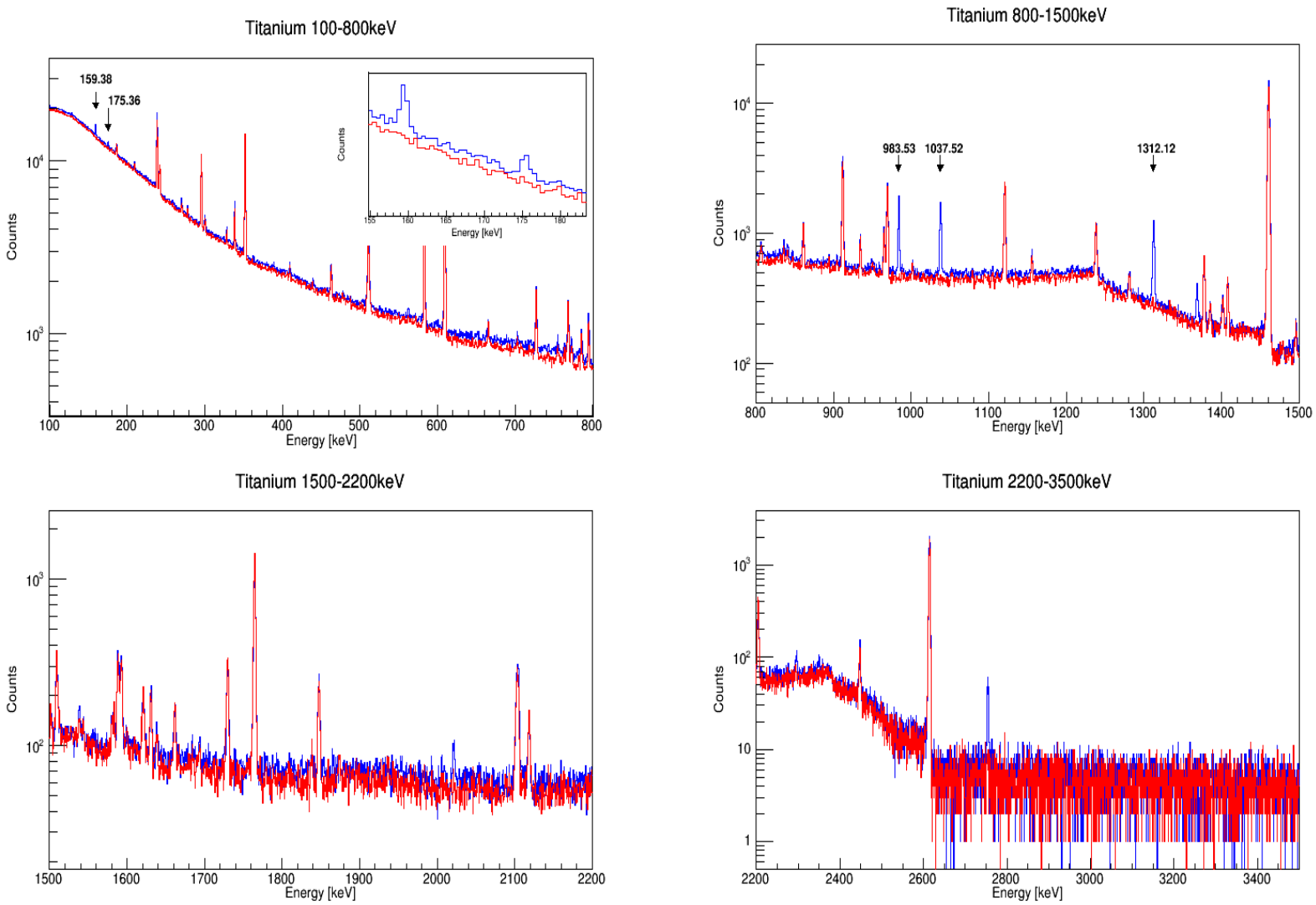


Figure 9. Titanium's 12-hour spectrum (blue) and the 12-hour background spectrum (red) is also shown for comparison.

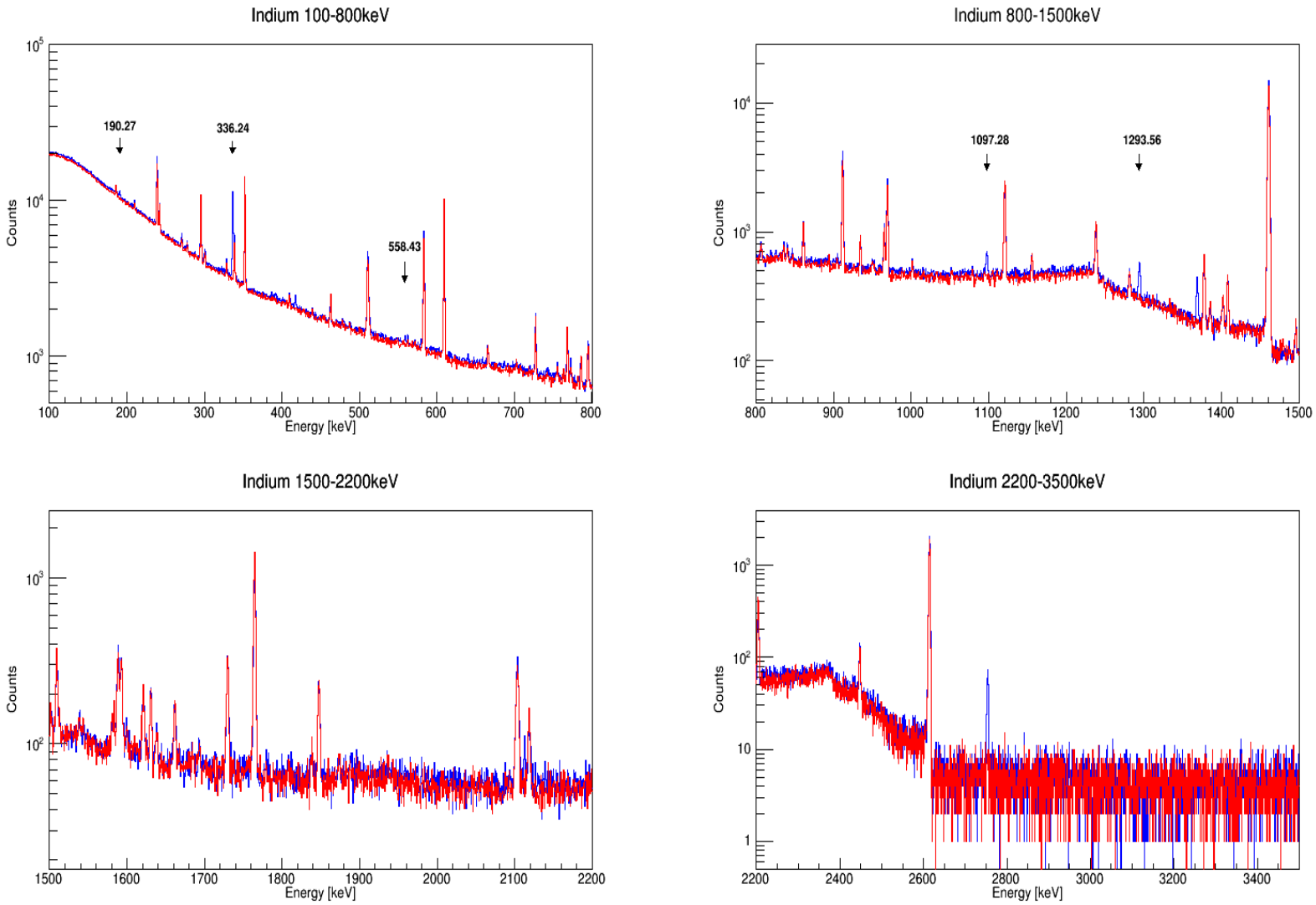


Figure 10. Indium's 12-hour spectrum (blue) and the 12-hour background spectrum (red) is also shown for comparison.

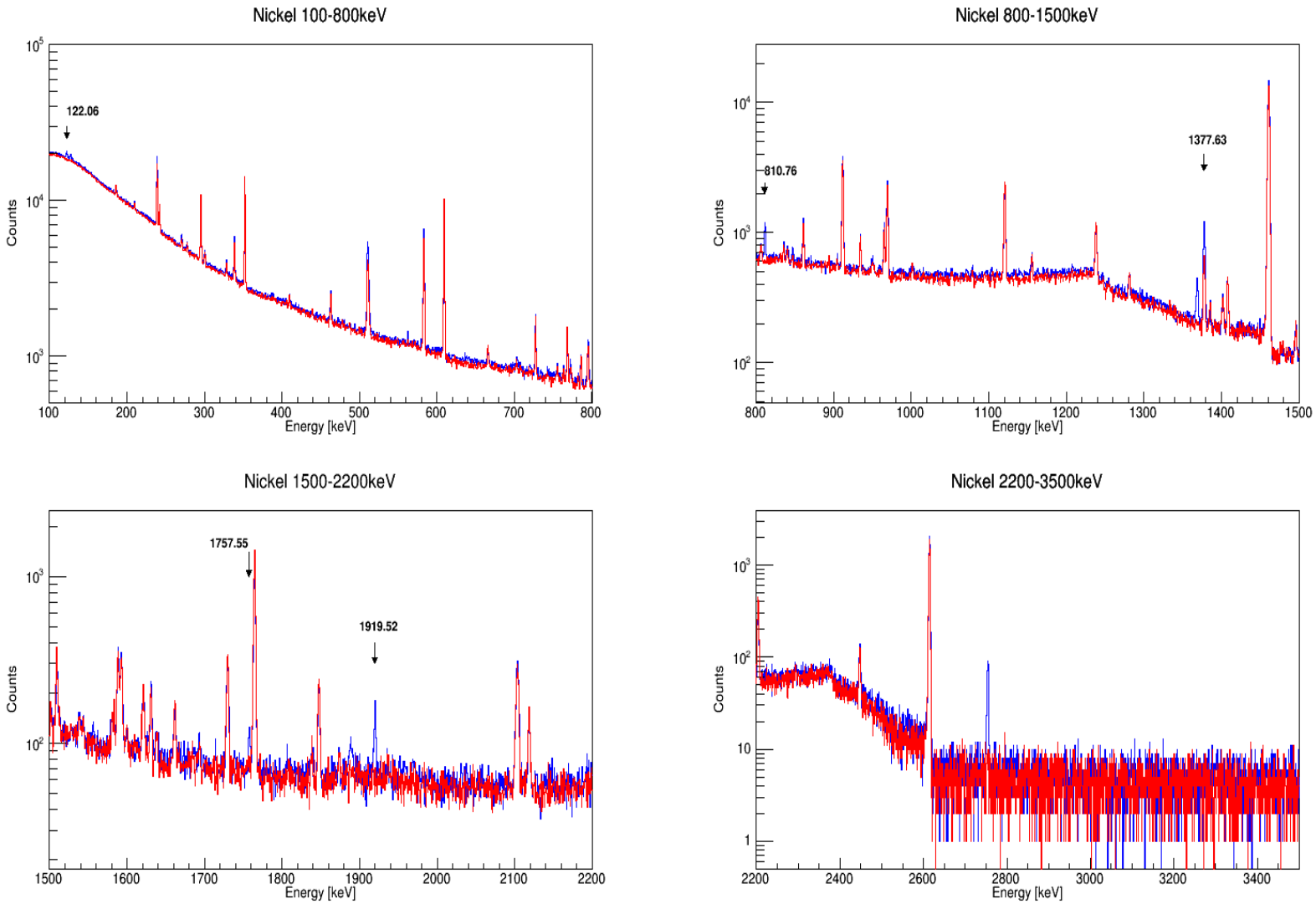


Figure 11. Nickel's 12-hour spectrum (blue) and the 12-hour background spectrum (red) is also shown for comparison.

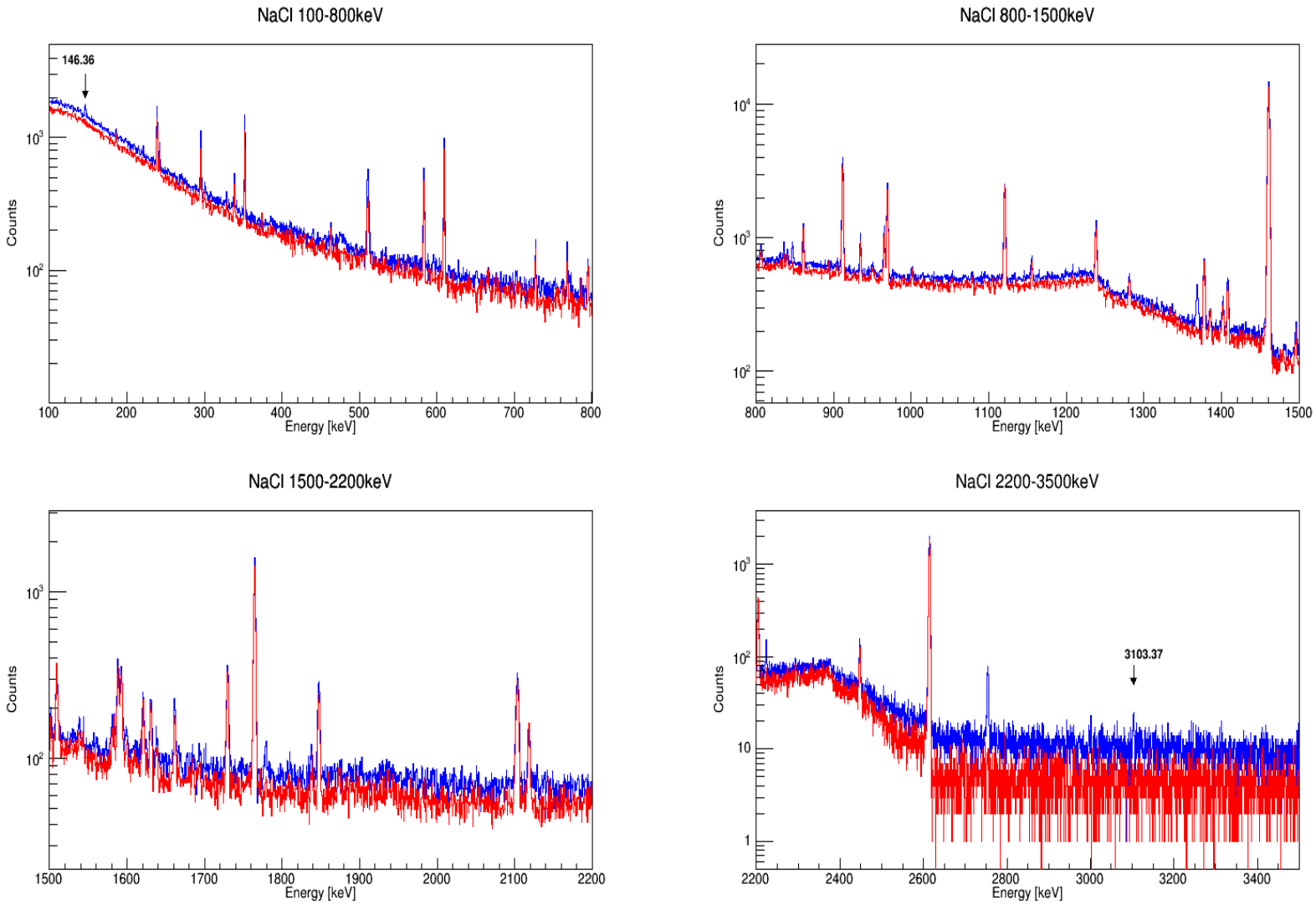


Figure 12. Sodium Chloride's 12-hour spectrum (blue) and the 12-hour background spectrum (red) is also shown for comparison. Sodium does not yield reaction products with half-lives long enough for activation analysis.

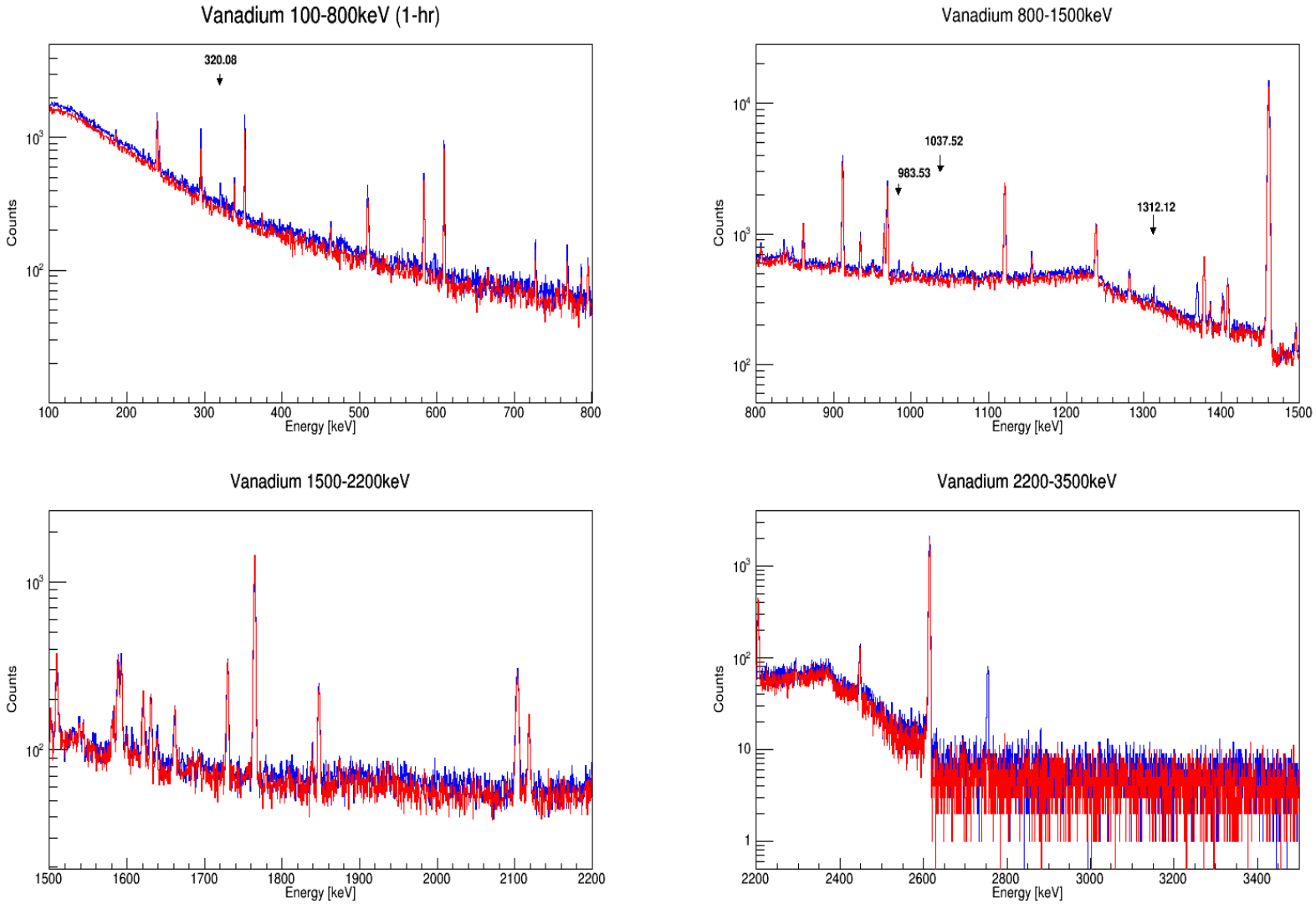


Figure 13. Vanadium's 12-hour spectrum (blue) and the 12-hour background spectrum (red) is also shown for comparison. For the top left spectrum, the first hour's spectrum and its corresponding background spectrum are shown to make the 320.08 keV peak visible.

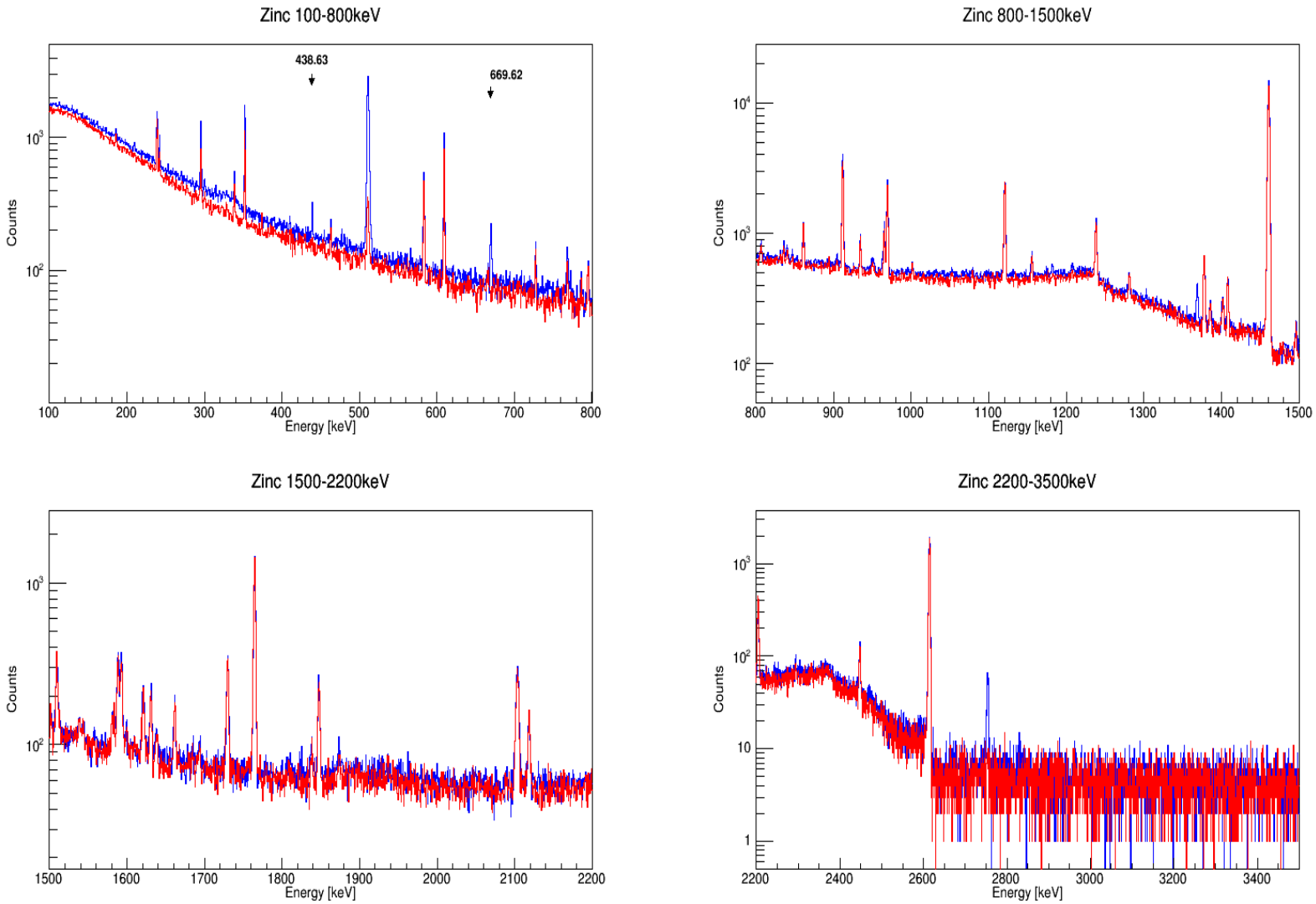


Figure 14. Zinc's 12-hour spectrum (blue) and the 12-hour background spectrum (red) is also shown for comparison.

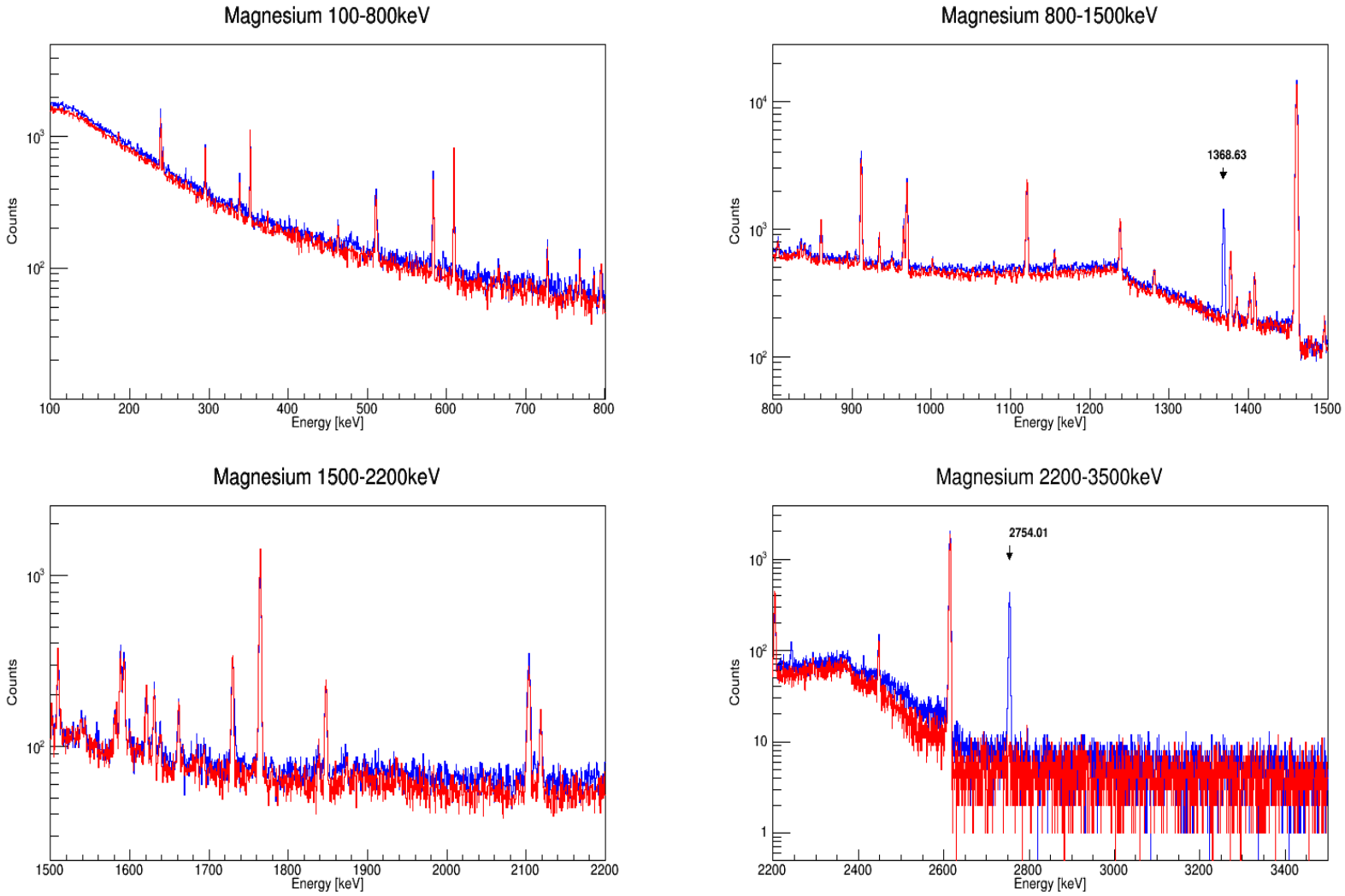


Figure 15. Magnesium's 12-hour spectrum (blue) and the 12-hour background spectrum (red) is also shown for comparison.

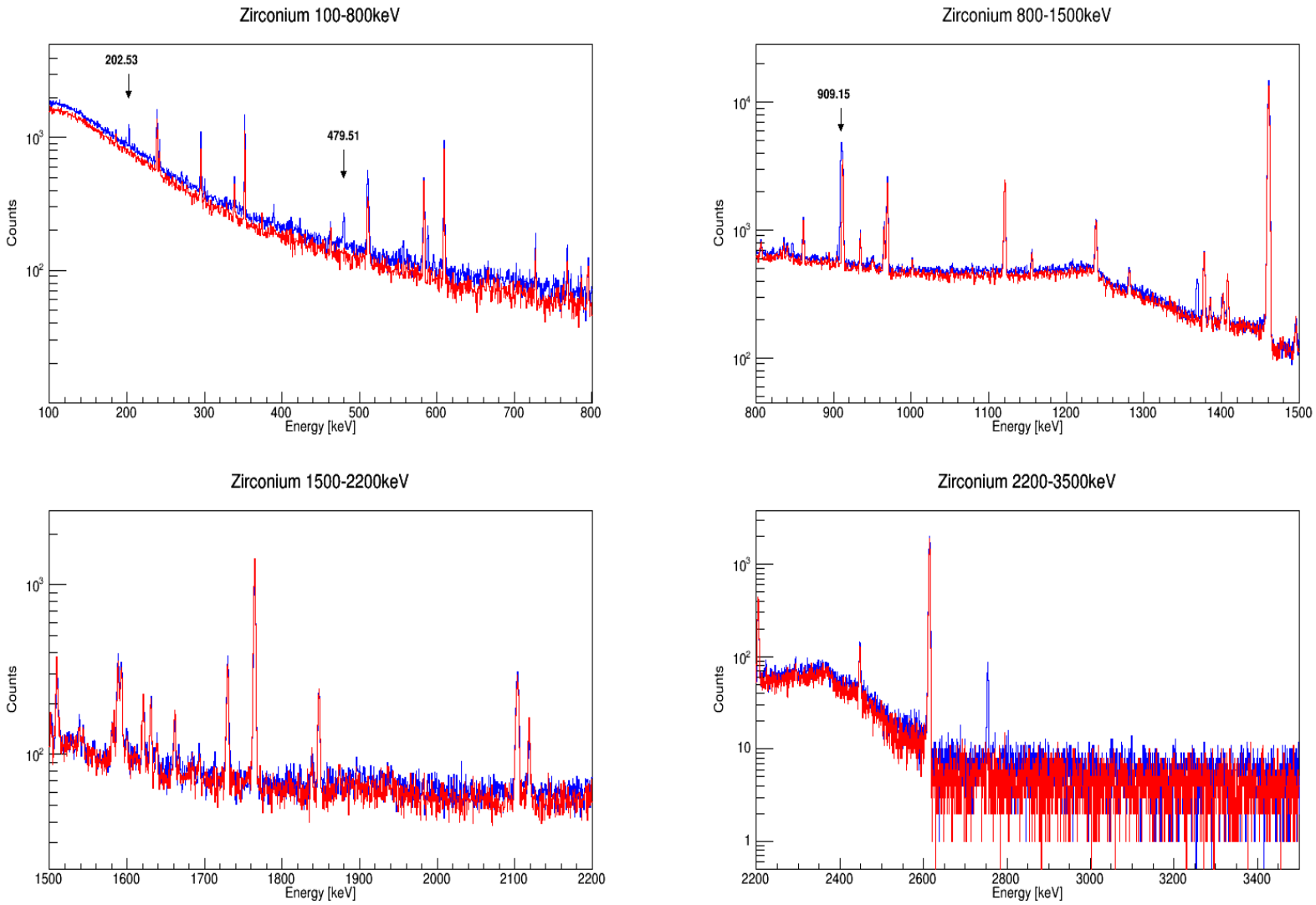


Figure 16. Zirconium's 12-hour spectrum (blue) and the 12-hour background spectrum (red) is also shown for comparison.

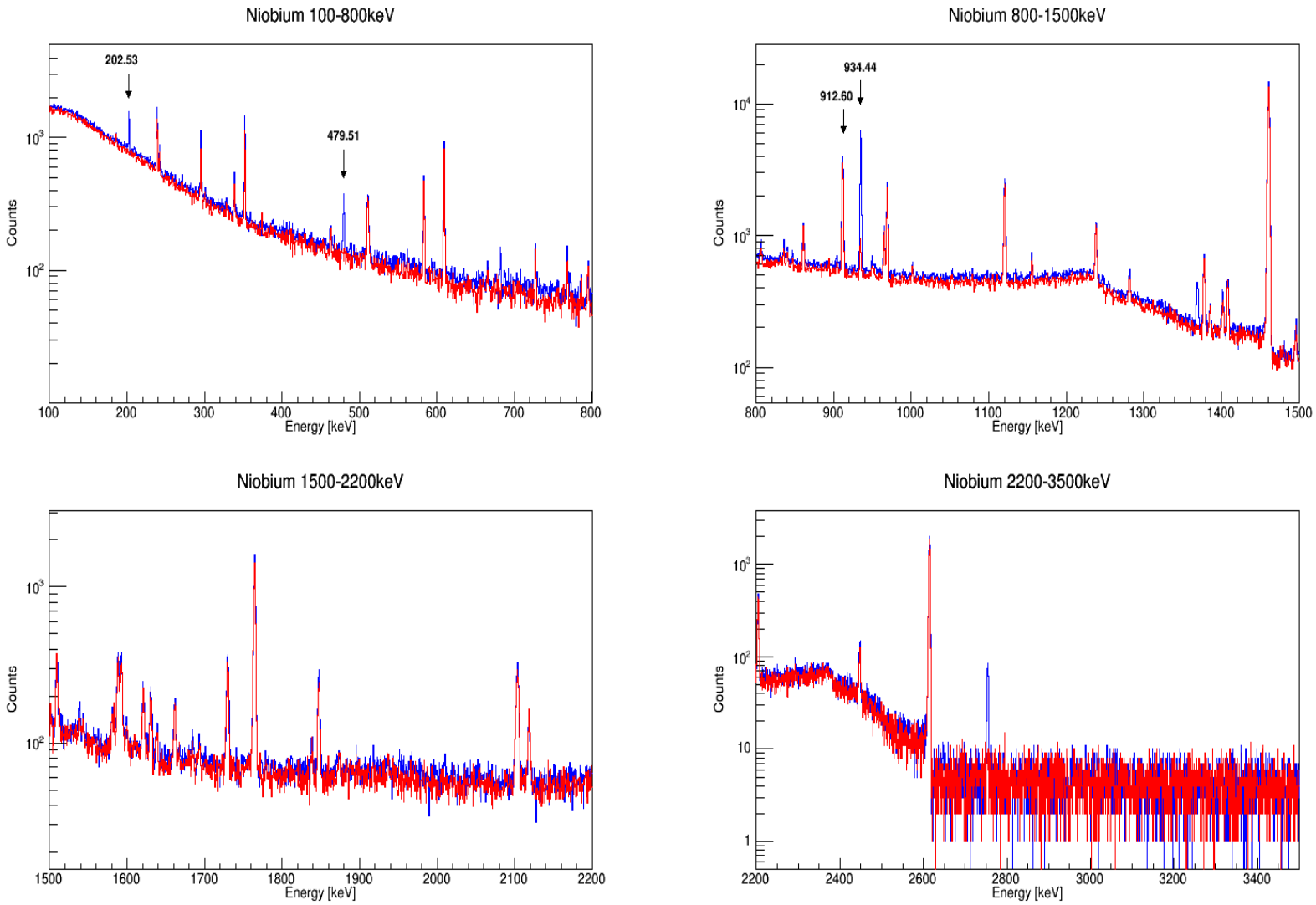


Figure 17. Niobium's 12-hour spectrum (blue) and the 12-hour background spectrum (red) is also shown for comparison.

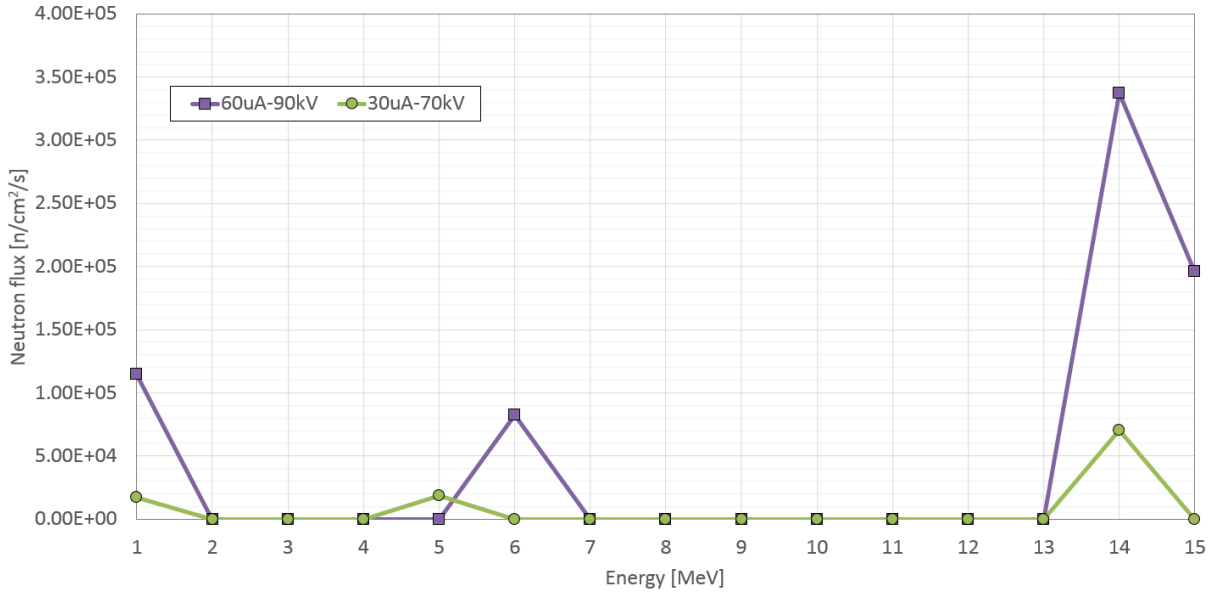


Figure 18. The determined neutron flux for each generator setting.

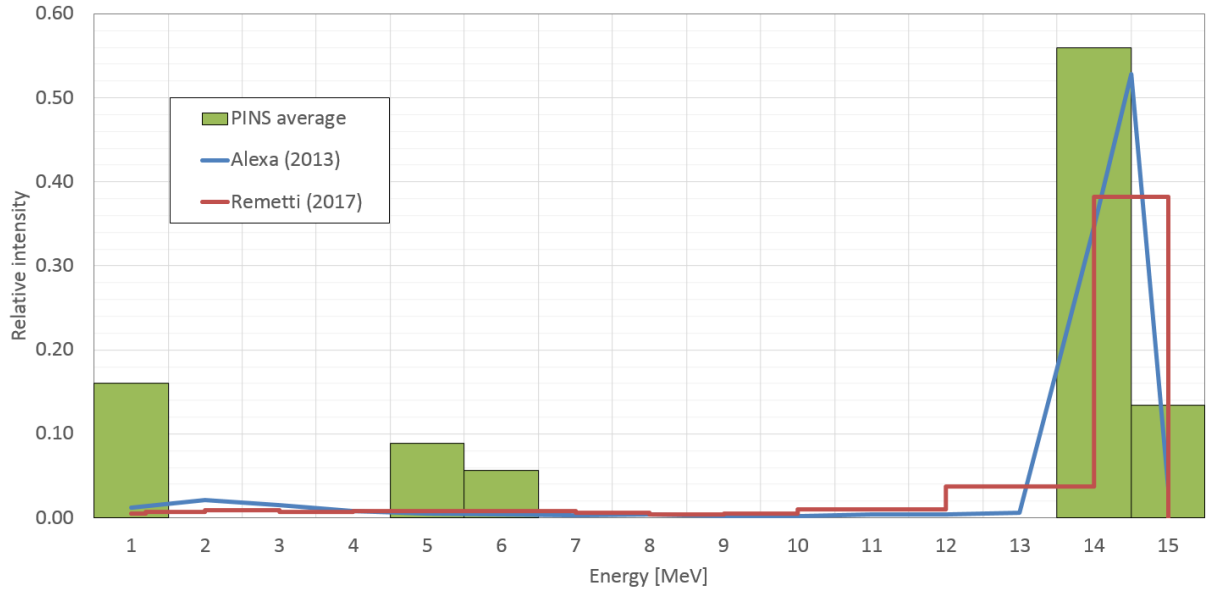


Figure 19. Normalized neutron fluxes for comparison. Simulated neutron fluxes from previous studies [Ale13, Rem17] using MCNP were compared to the average of normalized neutron fluxes shown in Figure 18.

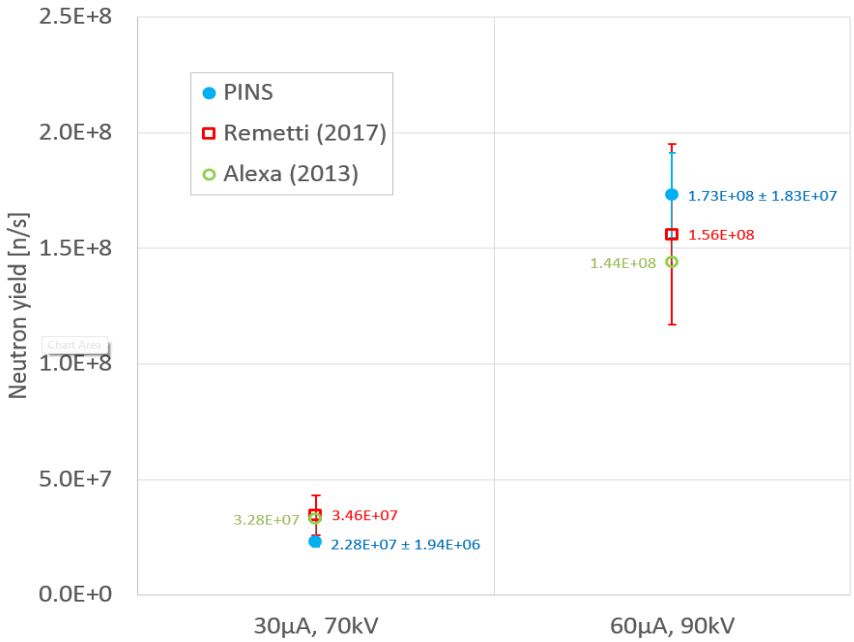


Figure 20. The determined Neutron yields for two generator settings. Neutron yields for the same setting from two references [Ale13, Rem17] are also shown for comparison.

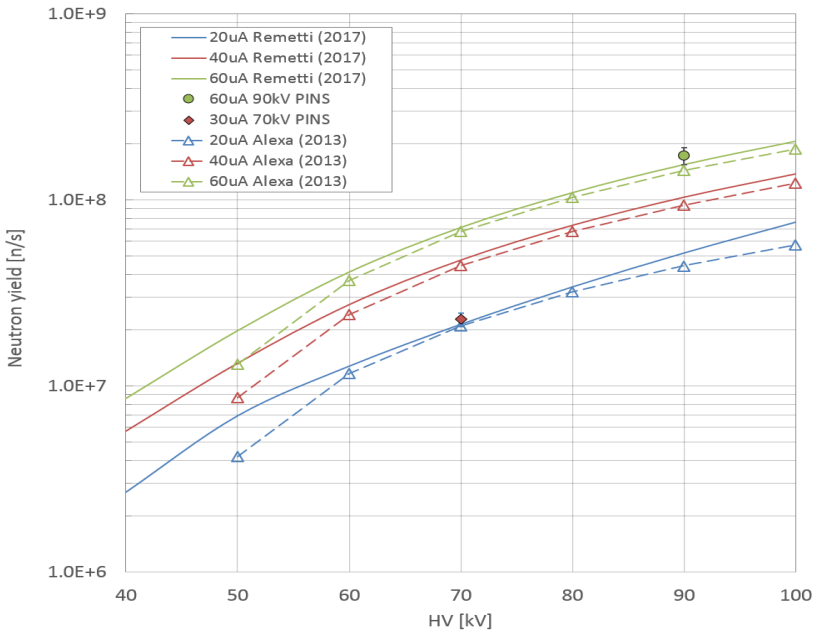


Figure 21. Empirical formulae (Equation ((*7*) and ((*8*)) to estimate neutron yields are plotted as functions of current and high voltage. For the plots of Alexa and Uhlář (2013), the duty factor of 1.0 was used. The Neutron yields determined in this study are also shown for comparison.

Figure 22. A BC400 plastic scintillator was used as an independent neutron flux monitor.

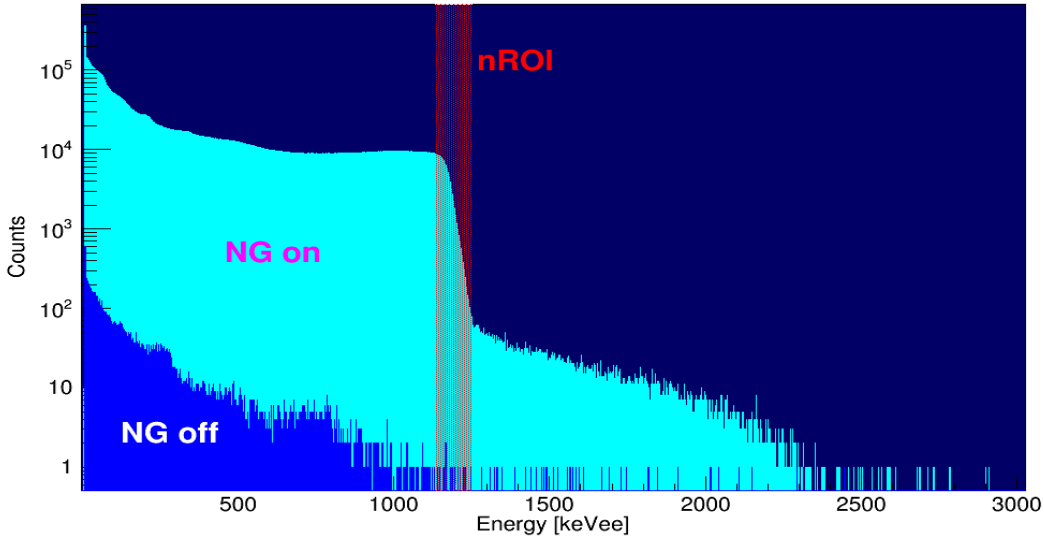


Figure 23. BC400 neutron spectrum. The cyan neutron spectrum was measured for 6 hours continuously while the generator was turned on and an Aluminum foil was being irradiated. The background spectrum (labeled "NG off") was collected for 6 hours while the neutron generator was turned off. It is very important to understand that old energy calibration parameters were used by default so that the energy scale in this figure is not correct. Also, energy calibration was typically done using gamma-ray peaks (keV electron equivalent or keVee) so that the energies in this figure are simply used to indicate the position of the nROI window. Total counts inside the nROI (from 1132 to 1248 keVee in this figure or raw channels from 2651 to 2921) could be useful to monitor neutron flux since the counts within this region are less sensitive to any induced gamma-rays by 14.1 MeV neutrons as suggested by Mitra and Wielopolski [Mit08].

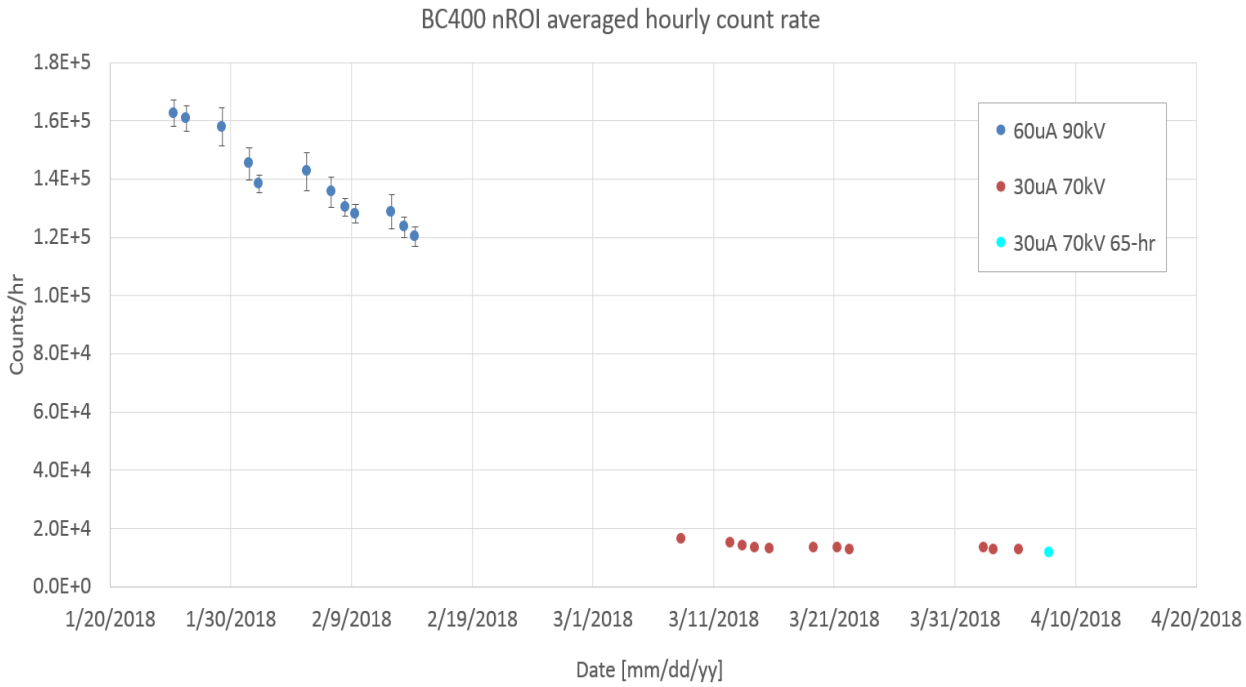


Figure 24. A time series of BC400 nROI hourly count rates. Irradiations under the high-yield and the low-yield settings were conducted over a two-month period. A 65-hour continuous operation of the same generator under the low-yield setting was performed after all irradiations were completed. The average count rates for two settings were $1.36\times10^5$ nROI counts/hour and $1.34\times10^4$ nROI counts/hour, respectively. There was noticeable decreases in the hourly count rates for the high-yield setting, and the standard deviation was found to be 10.6% of the average count rate. For the low-yield setting, the standard deviation was about 8.5% of the average.

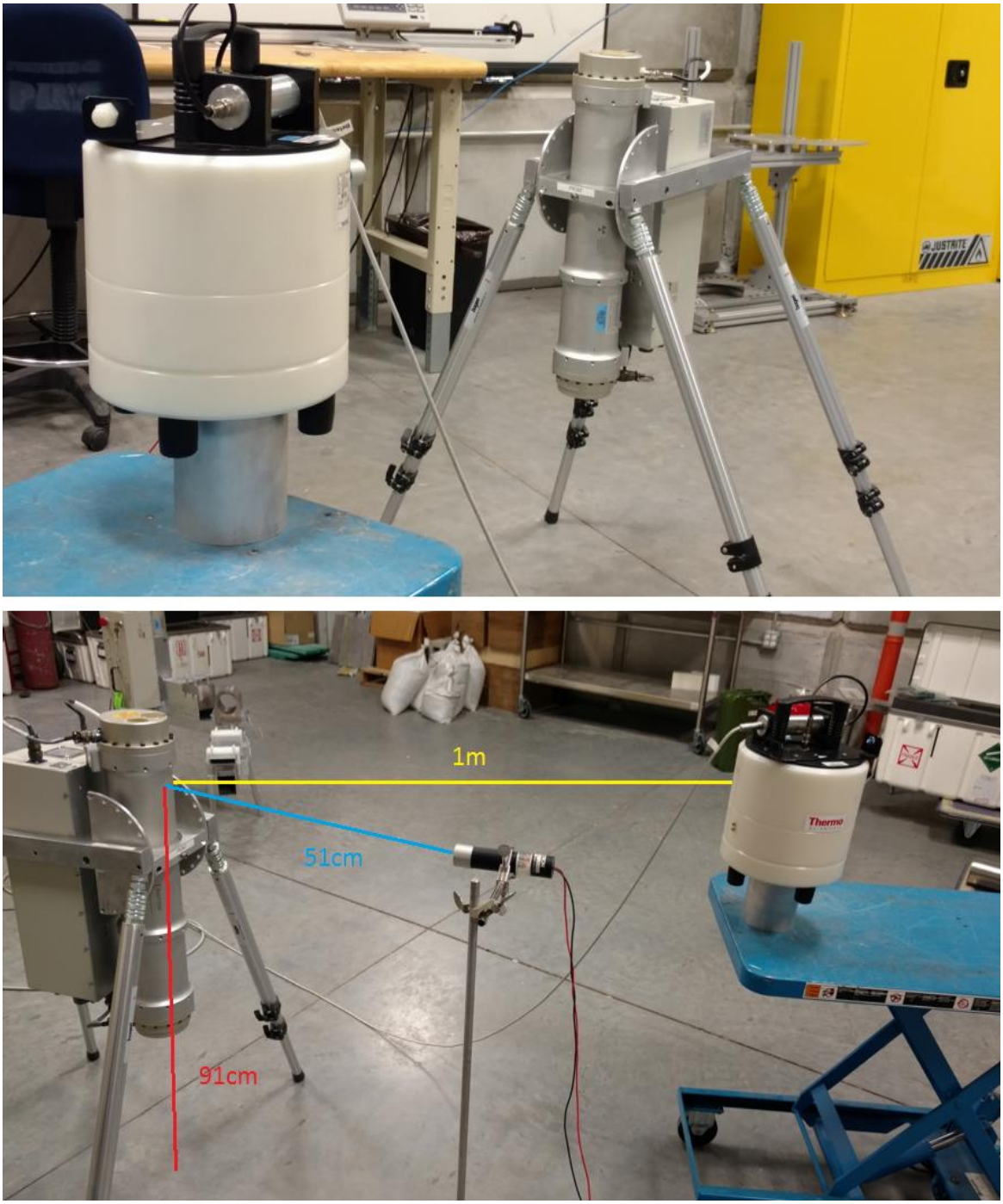


Figure 25. SWENDI-2 SETUP IN THE PINS LAB.

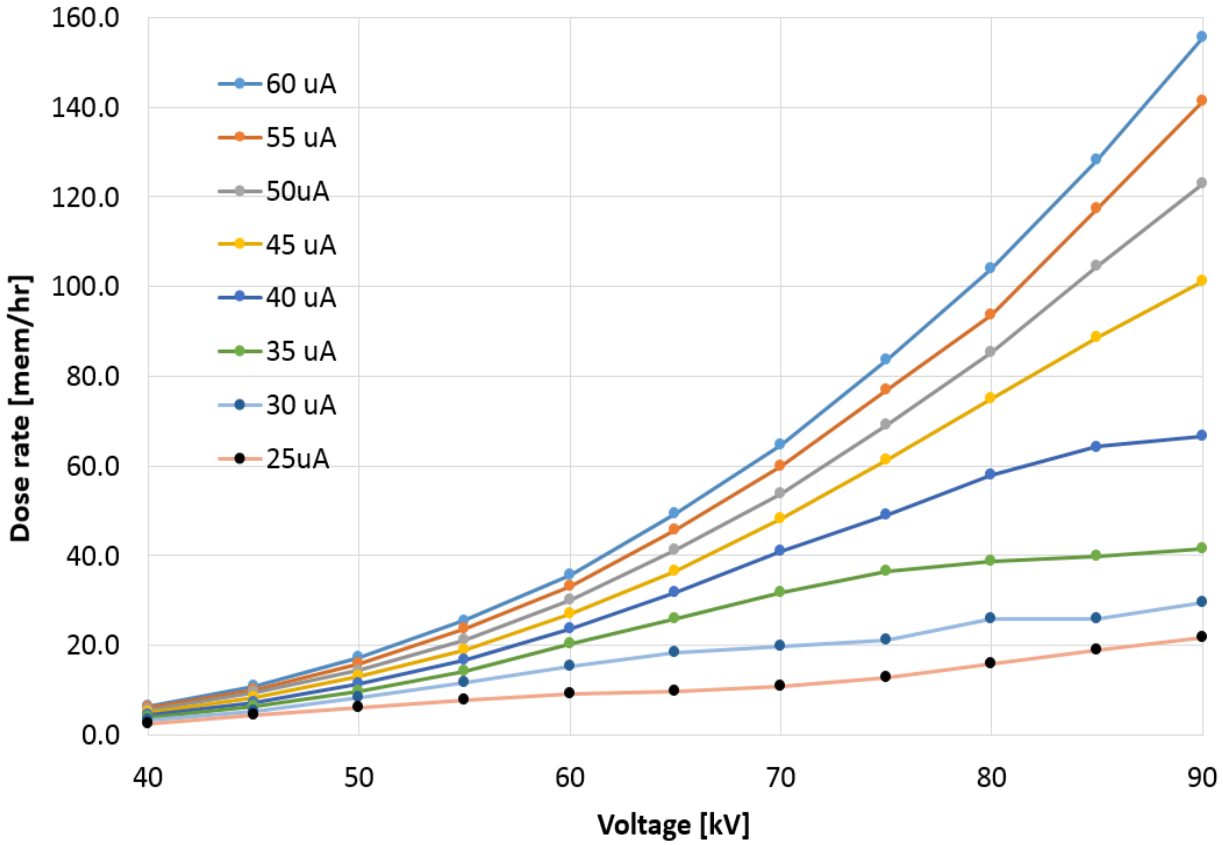


Figure 26. A plot of SWENDI-2 dose rate readings as a function of the MP320's voltage and current settings.